

# ELECTRON TRANSPORT THROUGH DOUBLE QUANTUM DOTS IN AN AHARONOV-BOHM RING

A THESIS

SUBMITTED TO THE GRADUATE SCHOOL  
IN PARTIAL FULFILLMENT OF THE REQUIREMENTS

FOR THE DEGREE

MASTER OF SCIENCE

by

CHUNGHEE ROH

ADVISOR: DR. ERIC R. HEDIN

BALL STATE UNIVERSITY

MUNCIE, INDIANA

NOVEMBER, 2008

## ABSTRACT

Quantum dots (QDs), which are formed by a double barrier resulting in resonant-state electrons, are one of the ideal experimental tools to confine electrons and to study the tunneling of an electron through a double barrier in a one-dimensional transmission channel. In our research, we have two laterally coupled QDs in an Aharonov-Bohm (AB) ring geometry in which the coupling between two dots can be controlled. We use the tight-binding model to compute the exact transmission amplitude of an electron through the discrete quasi-bound states in coupled QDs embedded in an AB ring. We study the effect of magnetic flux on the transmission as well as explore how the inter-dot coupling changes the resonant states in QDs. We confirm that the lead-dot couplings involve the lifetime of the quasi-bound states in a symmetrical interference experiment. By tracing the position of the resonances of quasi-bound states, we can predict the shift of bonding and antibonding states for both single and multiple state-identical QDs as a function of energy levels and inter-dot coupling parameters.

## ACKNOWLEDGEMENTS

I would like to thank to my advisor, Dr. Eric Hedin, who encouraged me to keep going on my research whenever I was discouraged on off-track.

I would also like to thank Dr. Yong Joe who motivated me with his perseverance and knowledge.

I would also like to thank Dr. Ronald Cosby for reading my thesis and for having given me the basic concepts of solid state physics.

I would also like to thank Dr. Thomas Robertson for reading my thesis and for his dedication as a chairperson.

Apart from the Department of Physics and Astronomy, I would like to thank Ko and Carlos for providing me with a shelter last summer.

I want to say ‘thank you’ to my parents, brother, and Meng for supporting and advising me. In the end, I would like to say goodbye to my grandpa.

# CONTENTS

	<u>Page</u>
ABSTRACT.....	i
ACKNOWLEDGEMENTS.....	ii
LIST OF FIGURES.....	v
CHAPTERS	
1. Introduction.....	1
2. Electron transport and resonance phenomena through QDs.....	3
2.1 Two dimensional gas.....	3
2.2 Phase difference in an Aharonov-Bohm ring.....	5
2.3 Conductance.....	7
2.4 Breit-Wigner and Fano resonances.....	8
3. The tight-binding model.....	14
3.1 Introduction.....	14
3.2 General formalism.....	16
3.3 Dispersion relation.....	20
3.4 Double barrier resonance tunneling in a 1D periodic lattice.....	21
3.5 Discrete energy state.....	26
3.6 The nearest-neighbor coupling effect.....	27
4. Electron transport in a double quantum dot.....	29
4.1 Intoroduction.....	29
4.2 Formalism.....	32
4.3 Aharonov-Bohm oscillations.....	36
4.4 Inter-dot coupling effect.....	42
4.5 Suppressed and maximized transmission.....	46

5. Transmission through multiple states in a coupled quantum dot.....	49
5.1 Introduction.....	49
5.2 Formalism.....	51
5.3 Identical quantum dots.....	53
5.4 Inter-dot coupling between the higher-level states, $v_{db}$ .....	55
5.5 Inter-dot coupling, $v_{ca}$ .....	58
5.6 Even-odd, odd-even coupling.....	59
6. Conclusion.....	62
7. References.....	64
8. Appendix <b>A</b> : Calculation of the transmission amplitude for single-state QD.....	67
9. Appendix <b>B</b> : Calculation on the transmission amplitude at $\epsilon_A=\epsilon_B$ .....	70
10. Appendix <b>C</b> : Calculation of the transmission amplitude at $(E, \epsilon_A, \epsilon_B) \rightarrow (0,0,0)$ .....	72
11. Appendix <b>D</b> : Calculation of the transmission probability for two states in a QD.....	74

## LIST OF FIGURES

<p>Figure 2.1 Conduction and valence band line-up at a junction between an n-type AlGaAs and intrinsic GaAs. (a) Before charge transfer, their band gaps are different. (b) When they are in contact, energy levels are re-arranged at the interface (x-y plane) in (b). Note that this is a cross-sectional view. Patterning is done on the surface (x-y plane) using lithographic techniques [11].....</p>	3
<p>Figure 2.2 The schematic Aharonov-Bohm effect experiment. An electron beam is coming from the left and splits into both sides of the solenoid. The vector potential due to a magnetic flux through the cylinder-like circle (dotted blue) makes a phase difference when it is recombined [14].....</p>	6
<p>Figure 2.3 (a) Ring measures the Aharonov-Bohm effect in solid conductors. A vector potential field due to a magnetic field (arrows) shifts the phase of the electron wave function and changes the ring's electric resistance, which is determined by measuring the voltage and current. (a)The AB effect accounts for the oscillation in the electrical resistance of the ring [15].....</p>	8
<p>Figure 2.4 Double barrier resonant tunneling shows a typical BW resonance (Eqs. (2.6) and (2.7)). (a) Transmission probability on the real-energy axis and (b) corresponding transmission amplitude in the complex-energy plane. The BW resonance has a peak at <math>E_p</math>.....</p>	10
<p>Figure 2.5 Eq. (2.13) is plotted as a function of <math>\epsilon</math> when <math>q</math> value is varied. The blue dashed line (<math>q=0</math>) is a Fano-dip type resonance while the red dashed line (<math>q=10</math>) is a BW type resonance. The black solid line (<math>q=1</math>) shows a typical Fano resonance.....</p>	12
<p>Figure 3.1 Schematic drawing of wavefunctions of electrons on two hydrogen atoms at large separation (upper). (a) Ground state wavefunction at closer separation (lower). (b) Excited state wavefunction (lower) [23].....</p>	15
<p>Figure 3.2 The 1s band of a ring of 20 hydrogen atoms; the one-electron energies are calculated in the tight-binding approximation with the nearest- neighbor overlap integral [23].....</p>	16
<p>Figure 3.3 One dimensional lattice in a crystal with a lattice spacing '<math>a</math>'. The atomic wave functions have such a short range that only nearest-neighbor terms are considered in a calculation, with overlap integral, <math>V_0</math> .....</p>	16
<p>Figure 3.4 The curve depicts a periodic potential structure down along a line of atomic sites. Two potentials around the origin are bigger than the others making a double barrier resonance structure.....</p>	21
<p>Figure 3.5 Transmission probability <math> t(E) ^2</math> (black dotted line) plus the reflection coefficient <math> r(E) ^2</math> (dashed orange line) is always 1 (solid red line) as expected. The black dotted symmetric line shows the BW resonance for double barrier resonant tunneling. This is plotted for <math>\bar{\epsilon}_0 = 0</math>, <math>V_0 = 1</math>, and <math>V_1 = 0.3</math> .....</p>	25

Figure 3.6 The transmission coefficient of a double barrier structure plotted as a function of incident energy  $E$ . Resonance poles depend on the quasi-bound state energy  $\bar{\varepsilon}_0$  of the symmetric double barrier. In (a),  $\bar{\varepsilon}_0 = -0.5$  (dotted line),  $0.5$  (solid line). In (b)  $\bar{\varepsilon}_0 = -1$  (dotted line),  $1$  (solid line),  $V_1 = 1$ , and  $V_0 = 0.3$ .....26

Figure 3.7 Transmission probability of a double barrier structure as a function of incident energy  $E$ . (a) The resonance gets wider as the nearest neighbor coupling  $V_1$  increases from the solid red line to outer -  $0.1$  (center),  $0.2$ ,  $0.3$ ,  $0.4$ , and  $0.5$  (outer line). (b) The solid red line indicates  $V_1 = 1.0$ .  $V_1$  increases from the center to outer (solid red line) -  $0.6$  (center),  $0.7$ ,  $0.8$ ,  $0.9$ ,  $1$  (solid red line). When  $V_1$  is equal to  $V_0$ , the transmission is '1' for all the regions of incident energy.....28

Figure 4.1 (a) Experimental layout from A. W. Holleitner *et al* [24]. Two QDs are formed within a 2DEG 90nm below the surface of an AlGaAs/GaAs heterostructure. Electrons tunnel via both dots from source to drain (black arrows). Coupling between the two dots (red arrow) is tuned by voltages applied to gate **A** and **B**. (b) AFM picture of the sample. The heights are color coded as indicated on the lower left. To define two QDs, negative voltages are applied to gates **A**, **B**, **1** and **2**. Both QDs are equally connected to drain and source contacts.....29

Figure 4.2 Conductance plots obtained from a double quantum dot at 815mK traced by cotunneling of the two binding electrons. The resonances 1 through 8 are picked at  $V_2 = -430$ mV when  $V_1$  is varied from  $-450$ mV to  $-460$ mV. Increasing the negative voltages applied to gate A and B from  $-279$ mV to  $-291$ mV raised the inter-dot tunneling barrier, which in turn suppresses all but one of the resonances. The data are presented with an offset for better visibility [24].....30

Figure 4.3 A schematic of Aharonov-Bohm ring. Two QDs are weakly coupled with  $v_j$ . A magnetic field perpendicular to the ring is applied.....31

Figure 4.4 Phase difference from the lattice point at  $n = -1$  to another dot at  $n = 1$  is  $\varphi$  in an AB ring. Minus signs are for the clockwise traversals and plus signs for counter clock-wise motion. The total phase difference is the sum of the absolute value of each phase factor (Eq. (4.3)).....34

Figure 4.5 Transmission coefficient (dashed orange) plus reflection coefficient (dashed black) is always '1' (solid orange):  $T + R = 1$ . This is plotted at  $V_1 = 0.3$ ,  $\varepsilon_A = 0.5$ ,  $\varepsilon_B = -0.5$ ,  $v_j = 0$  and  $\varphi = 0$  which means there is no dot-dot interaction and no magnetic flux through the AB ring.....35

Figure 4.6 (a) The same experimental setup as in Fig. 4.1(b) by Holleitner *et al.* [7]. Gates 3,4 (above) correspond to gate 2 in Fig. 4.1(b). Gate 5 is matched with gate 1 in Fig. 4.1(b). The circles indicate the two quantum dots within the 2DEG (b) The device operates as an AB interferometer. If a magnetic field is applied perpendicular to the QDs, the amplitude of the source-drain current (gate **1** and **2**) at the crossing points produces oscillations periodic with the magnetic field (inset) [7].....36

Figure 4.7 Transmission probability as a function of the magnetic flux for fixed incoming electron energies. (a)  $E=0$ . (dotted), 0.25 (dashed), 0.5 (solid) and (b)  $E=0.75$  (dotted), 1.0 (dashed), 1.25(solid line) for  $v_j=0$ ,  $\varepsilon_A =0.5$ ,  $\varepsilon_B =-0.5$ , and  $V_1=0.3$ .....37

Figure 4.8 Suppressed transmissions occur at integer  $\Phi/\Phi_0$  when incident energy approaches to the average of two QD energy values. In each case  $E = (\varepsilon_A + \varepsilon_B)/2$ , The shape of transmission of (c) is identical to (d). These are all plotted at  $v_j = 0, V_1 = 0.3$ .....38

Figure 4.9 Identical AB oscillations of the transmission at  $E = \bar{\varepsilon}$  for some QD energy level difference. The QD parameters are changed from (a) to (d):  $(E, \varepsilon_A, \varepsilon_B) \rightarrow$  (a) (0.3,0.2,0.4), (b) (0.2, 0.1, 0.3), (c) (0.1, 0, 0.2), (d) (0, -0.1, 0.1).....39

Figure 4.10 In contour plots of  $T(E, \varphi)$  the color scale indicates the magnitude of the transmission. The shape of two contours is identical except that the line of symmetry is shifted as two quasi-bound states are slightly changed from (a)  $\varepsilon_A = 0.1, \varepsilon_B = -0.1$  to (b)  $\varepsilon_A = 0.4, \varepsilon_B = 0.2$  .....40

Figure 4.11 Schematic picture of total reflections when the magnetic flux  $\Phi/\Phi_0=0$  or integer and the incident energy meets the average energy value of the two dots. ....42

Figure 4.12 For the ring with symmetric arms in the absence of magnetic flux, the position of the resonance zero is given by  $E_0 = (\varepsilon_A + \varepsilon_B)/2 + v_j$ . Inter-dot coupling is varied from (a) to (d): (a) 0, (b) 0.1, (c) 0.2 and (d) 0.5. The other QD parameters are fixed at  $V_1 = 0.3, \varepsilon_A = 0.5, \varepsilon_B = -0.5$ , and  $\Phi = 0$ . ....43

Figure 4.13 As  $v_j$  increases the lattice-like resonance loses intersection domains. From (a) to (d),  $v_j$  is increased:  $v_j =$  (a) 0, (b)0.25, (c) 0.5, (d) 0.75. Other parameters are fixed at  $E=0, V_1=0.3$ , and  $V_0=1$ .....44

Figure 4.14 (a) Scanning electron micrograph of parallel double QDs. The lithographic size of each dot is 170nm $\times$ 200nm. (b) Logarithm of double QD conductance as a function of  $V_2$  and  $V_4$  with different couplings. The inter-dot coupling is increased from (1) to (4).....45

Figure 4.15 (a) AB oscillations are repeated every integer for  $v_j=0$ . (b) The periodicity of AB oscillations is changed to two flux quantum with a finite inter-dot coupling:  $v_j=0.3$ . The other QD parameters are fixed at  $E=0, V_1=0.3$ , and  $V_0=1$  for identical QD ( $\varepsilon_A=\varepsilon_B=0$ ).....46

Figure 4.16 At fixed  $\varepsilon_B$ , the Fano resonance is observed because of the suppressed transmission along the yellow line of  $\bar{\varepsilon} = \varepsilon_A + \varepsilon_B = 0$ . Two plots above are generated for the case with symmetric arms,  $V_1=0.3$ . For (b),  $\varepsilon_B$  is fixed at 0.1 and  $V_0=1$ . QD parameters are applied to both (a) and (b) :  $v_j=0, E=0$ , and  $\Phi=0$ .....47

Figure 4.17 (a) The Fano dip-peak is changed to a peak-dip pair (b) in the Fano resonance as one of the dot energies is changed: (a)  $\epsilon_B = 0.2$  and (b)  $\epsilon_B = -0.2$ .....48

Figure 5.1 Schematic of the two energy states in double quantum dots. Each state is coupled to other states with different coupling strengths. In addition to the magnetic flux  $\Phi$  threading the AB ring, the relevant coupling parameters between sites are defined.....50

Figure 5.2 Each resonant state represents four quasi-bound states with the conditions of  $V_1 = 0.3$ ,  $\Phi = 0$ , no inter-dot couplings ( $v_{da} = v_{db} = v_{cb} = v_{ca} = 0$ ), and ( $\epsilon_a = 0.5$ ,  $\epsilon_b = -0.2$ ,  $\epsilon_c = 0.1$  and  $\epsilon_d = 0.4$ ).....52

Figure 5.3 Resonance peaks through two identical quantum dots ( $\epsilon_d = \epsilon_b = 0.2$ ,  $\epsilon_c = \epsilon_a = -0.2$ ) in a symmetric AB ring in the absence of magnetic field are shifted to lower energy as all inter-dot couplings ( $v_{db} = v_{da} = v_{cb} = v_{ca} = v_j$ ) are simultaneously increased while the transmission zero,  $E_0$ , remains the same, despite the interaction between quasi-bound states ( $V_0 = 1$ ,  $V_1 = 0.3$ ,  $\Phi = 0$ ).....54

Figure 5.4 For the case with  $V_1 = 0.3$ ,  $\Phi_0 = 0$  and inter-dot couplings ( $v_{da} = v_{db} = v_{cb} = v_{ca} = v_j = 0.2$ ), as two bound state energies are varied: ( $\epsilon_a, \epsilon_b$ )  $\rightarrow$  (a)  $(-0.2, 0.2)$ , (b)  $(-0.4, 0.2)$ , (c)  $(-0.4, 0.1)$ , (d)  $(-0.4, 0.4)$ ,  $E_0$  depends only on two bound state energies,  $\epsilon_a$  and  $\epsilon_b$ .....55

Figure 5.5 Transmission plots with the increase of  $v_{db}$  from black, blue, red, and orange (right to left for  $E > 0$ ) with (0, 0.2, 0.4, 0.6). Other couplings are zero ( $v_{da} = v_{cb} = v_{ca} = 0$ ).....57

Figure 5.6 Transmission probability as a function of the incident energy for various  $v_{ca}$  black, blue, red and orange (0, 0.2, 0.4, and 0.6) for  $v_{da} = v_{db} = v_{cb} = 0$ .....59

Figure 5.7 Even-odd interaction creating the other peaks indicates that additional bound states are formed, while the two peaks at 0.2, -0.2 remain the same. Other inter-dot couplings besides  $v_{cb}$  are fixed at zero in the absence of magnetic flux.....60

## CHAPTER 1: Introduction

The quantum physics of resonant tunneling has attracted the attention of many physicists working in the mesoscopic world. Advances in nanotechnology have made it possible to fabricate a two dimensional electron gas (2DEG) at the interface of an AlGaAs/GaAs heterostructure. In this structure, it is possible to precisely study the transmission of resonant tunneling through quasi-bound states in a quantum dot (QD). A QD is often referred to as an artificial atom because electronic states within closed dots are quantized like a real atom [1-2]. One of the main features of transport through QDs is that the coherence of electrons is largely preserved, as manifested in phenomena such as the Aharonov-Bohm (AB) oscillations in multiply connected geometries [3]. A. Yacoby *et al.* were the first to show that the presence of quantum coherence in a mesoscopic system is detectable through interference in a two-terminal AB interferometer [1]. Keeping the transmission phase of one path constant (reference path), the phase change of the other can be measured [4]. The phase change across a transmission peak is expected to change by  $\pi$  in a two-terminal system [5], but the presence of magnetic flux through the AB-ring can modulate the quantum interference between those electron paths that encircle the ring and those that do not [6].

We analyze the novel quantum transmission through parallel-coupled double QDs in an AB ring by employing an exactly solvable tight-binding formalism. Via this novel experiment the dots are defined by independently tunable gates on a GaAs/AlGaAs

heterostructure containing a 2DEG typically located 80~100 nm below the surface [7]. Electron transport can be measured experimentally by detecting the current between drain and source. We solve for the transmission coefficient,  $T$ , which is simply related to the conductance,  $G$ , in a two-terminal device:  $G = 2e^2/h$  ( $e$  is electron charge and  $h$  is a Planck constant).

In chapter 2, we study the fundamental concepts of this research such as QDs within a 2DEG, the AB effect, and Breit-Wigner and Fano resonances [8-10], which are helpful to understand when studying the transmission of electrons. In chapter 3, we deal with the tight-binding model to derive the main equation for this thesis. In addition, we take a look at the electron transport in a one dimensional periodic lattice to explore the basic concept of the transmission through quasi-bound states confined in a double barrier. Next we move on to chapters 4 and 5 which contain most of the results for this research. In chapter 4, we study the transmission through the single quasi-bound states in double QDs embedded in an AB ring [11]. In the absence of magnetic flux and inter-dot coupling, we find that suppressed transmission ( $T=0$ ) occurs when the incident energy of an electron approaches the average value of the energies of the two dots [3]. We also study the effect of inter-dot coupling on the transmission. In chapter 5, we focus on the inter-dot coupling effects for multiple states through coupled identical double QDs, in contrast to a singular state which is studied in chapter 4.

## CHAPTER 2: Electron transport and resonance phenomena through QDs

### 2.1 Two dimensional electron gas

Recent work on electron tunneling through QDs has largely been based on GaAs/AlGaAs heterojunctions [12] where electrons are confined in a thin two-dimensional conducting layer (Fig. 2.1). In general, a heterostructure consists of two or more semiconductors with band gaps, which are combined in a single crystal [13]. With a correct layer and doping sequence one can create a triangular potential well along the  $z$ -direction below the surface. To understand how this layer is formed, we need to consider the conduction and valence band line-up in the  $z$ -direction when we first bring the layers in contact (Fig. 2.1(a)).

GaAs and AlGaAs are ideal candidates for the fabrication of heterostructures because they have almost the same lattice constants but different band gaps<sup>1</sup> [12]. The band gap of AlGaAs is wider than that of GaAs, and the Fermi energy  $E_F$  in the wide gap is higher than that in the narrow gap. When they are in contact, at the interface there is a discontinuity in the conduction and the valence band. The conduction band of the intrinsic semiconductor is bent down and the conduction band of the doped material is bent up. It looks like a well which goes below the Fermi energy so that electrons are piled up at the interface. The triangular shape is so narrow that the degree of freedom for electrons is in the plane of the interface. In equilibrium,  $E_F$  is constant over the whole

---

<sup>1</sup>  $a_{GaAs} = 5.6533 \text{ \AA}$  and  $a_{AlAs} = 5.6611 \text{ \AA}$ .

crystal. Now they are in the two-dimensional world, which is referred to as the two-dimensional electron gas (2DEG).

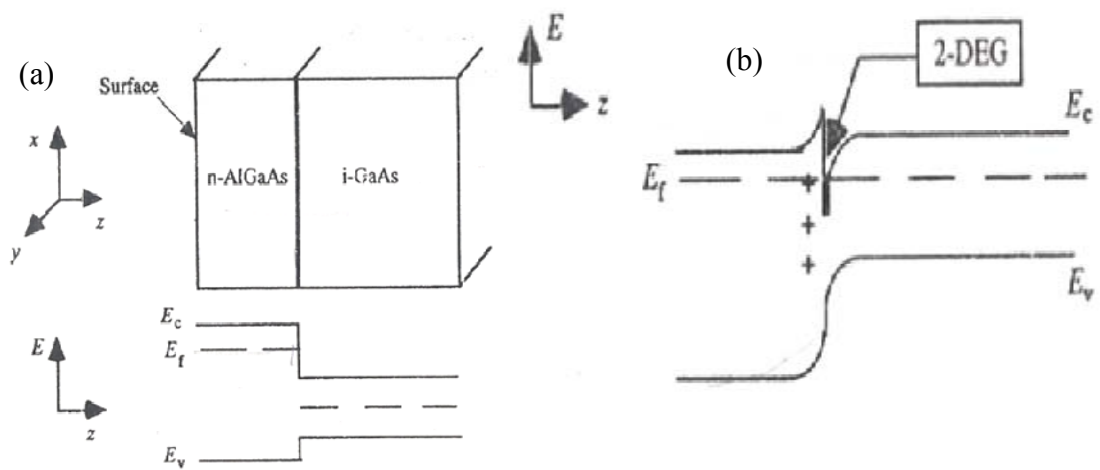


Figure 2.1. Conduction and valence band line-up at a junction between an n-type AlGaAs and intrinsic GaAs. (a) Before charge transfer, their band gaps are different. (b) When they are in contact, energy levels are re-arranged at the interface (x-y plane). Note that this is a cross-sectional view. Patterning is done on the surface (x-y plane) using lithographic techniques [13].

## 2.2 Phase difference in an Aharonov-Bohm ring

In classical electrodynamics, the potentials are not directly measurable and for a long time it had been believed that there could be no electromagnetic influences in regions where  $\mathbf{E}$  and  $\mathbf{B}$  are zero. But in 1959, Aharonov and Bohm designed an experiment to show that the vector potential could affect the quantum behavior of a charged particle even when the electrons are traveling in a region of zero magnetic field [6]. We'll derive in this section the Aharonov-Bohm (AB) effect and shows a basic example visually.

Assume that there is a particle in circular motion around a solenoid carrying steady current  $I$  (Fig. 2.2). If the solenoid is extremely long, the magnetic field inside it is uniform, and the field outside is zero. But the vector potential outside the solenoid is not zero due to this equation:  $\vec{B} = \vec{\nabla} \times \vec{A}$ . We can find the magnetic flux through the solenoid by using  $\mathbf{B}$ :

$$\Phi = \oint_{\text{surface}} \vec{B} \cdot d\vec{a} = \oint_{\text{surface}} (\vec{\nabla} \times \vec{A}) \cdot d\vec{a} = \oint_{\text{line}} \vec{A} \cdot d\vec{l} , \quad (2.1)$$

$$\Phi = 2\pi r A . \quad (2.2)$$

The vector potential,  $\mathbf{A}$ , has a direction,

$$\vec{A} = \frac{\Phi}{2\pi r} \hat{\phi} \quad (r > a), \quad (2.3)$$

where ' $a$ ' is the radius of the circle (blue dotted lines in Fig. 2.2).

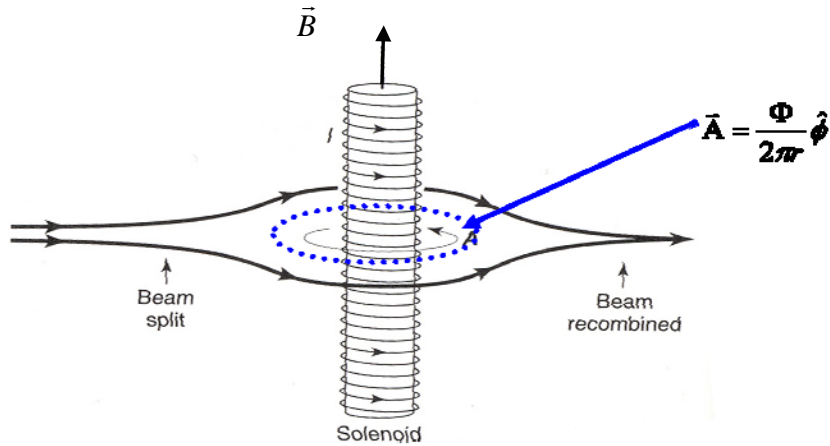


Figure 2.2 The schematic Aharonov-Bohm effect experiment. An electron beam is coming from the left and splits around both sides of the solenoid. The vector potential due to magnetic flux through the cylinder-like circle (dotted blue) makes a phase difference when the electron beams are recombined [14].

A beam of electrons is split in two and passed on either side of a long solenoid where it doesn't encounter the magnetic field. However, due to the non-zero vector potential of the magnetic flux, the two beams arrive out of phase by the factor:

$$\text{phase difference} = \frac{e\Phi}{\hbar} = \frac{e\Phi}{h/2\pi} = \frac{2\pi}{h/e} \Phi = 2\pi \frac{\Phi}{\Phi_0} \quad , \quad (2.4)$$

where  $\Phi_0$  denotes the flux quantum ( $h/e$ ). Notice that Eq. (2.4) implies periodicity.

When the magnetic flux is a multiple of  $h/e$ , the phase difference is always  $2n\pi$  where  $n$  is an integer. Many studies related to AB oscillations have shown this periodicity, later in this thesis, we will show it as well.

## 2.3 Conductance

In order to measure electron-interference effects in solid conductors, the quantum mechanics of electron waves must be translated to physical quantities that can be measured. Imry *et al.* introduced an experiment to show the AB effect by measuring the resistance between a metal ring (Fig. 2.3) [15]. Landauer in 1957 showed through his works [16] that the conductance  $G$  (inverse of the resistance) of a large macroscopic conductor is approximately proportional to the transmission probability divided by a fundamental quantum unit of resistance which is equal to Planck's constant divided by the charge of an electron squared:

$$G = \frac{2e^2}{h} T(\varepsilon_F) . \quad (2.5)$$

As a result of the AB effect, the electrical resistance of metal ring would oscillate periodically as a magnetic field applied to the center of the ring varied smoothly (Fig. 2.3(b)). This is due to the interference effect which manifests in the transmission,  $T$ , as a result of the wavefunction accumulating opposite phase shifts in each arm of the ring as a function of the external flux.

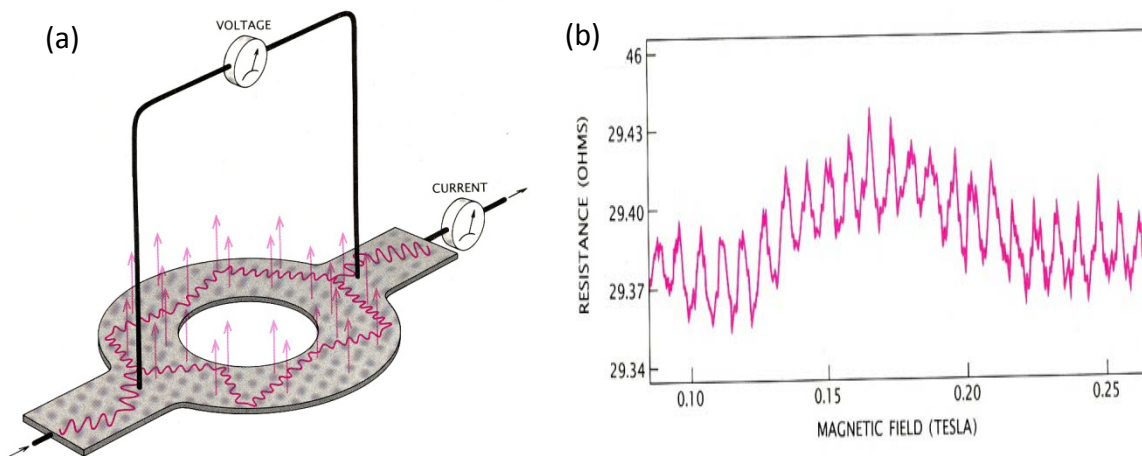


Figure 2.3 (a) Ring measures the Aharonov-Bohm effect in solid conductors. A vector potential field due to a magnetic field (arrows) shifts the phase of the electron wave function and changes the ring's electric resistance, which is determined by measuring the voltage and current. (a)The AB effect accounts for the oscillation in the electrical resistance of the ring as a function of magnetic flux [15].

## 2.4 Breit-Wigner and Fano resonances

Before dealing with the transmission phenomena, we need to study tunneling resonances. For double barrier resonant tunneling, it is well known that resonant-transmission phenomena are related to the quasi-bound states of the system [17-20]. According to the Breit-Wigner (BW) theory, the transmission amplitude in the complex-energy plane possesses a pole for each quasi-bound state [18, 19]. For an isolated pole at complex energy ( $E_p - i\Gamma$ ), the transmission amplitude can be written as

$$t(E) = \frac{i\Gamma}{E - (E_p - i\Gamma)}, \quad (2.6)$$

where  $E$  is the electron energy,  $E_p$  is the real energy part of the pole energy, and  $\Gamma$  is the half-width at half-maximum or the negative of the imaginary part of the pole energy. Then, the transmission probability  $T(E) = |t(E)|^2$  for physical energy on the real energy axis  $E$  is then given by

$$T(E) = \frac{\Gamma^2}{(E - E_p)^2 + \Gamma^2}. \quad (2.7)$$

Eq. (2.7) describes a transmission resonance with a Lorentzian line shape, and is shown in Fig. 2.4(a). The complex transmission amplitude is shown in Fig.2.4(b). Notice that BW formulation is no longer valid when more than one quasi-bound state is present [18].

When we consider an AB ring structure with more than one transmission pathways, the possibility of a Fano resonance arises. The Fano resonance is a manifestation of interference between the localized quasi-bound states of the QD in one arm and the continuum states in the other arm, characterized by both complete transmission and complete reflection [19]. The Fano resonance is noted for its asymmetrical line shape, while a BW resonance is totally symmetric. Z. Shao *et al.* demonstrated in Ref. [18] that an asymmetrical transmission line shape in the vicinity of a quasi-bound state is well described by the following equation:

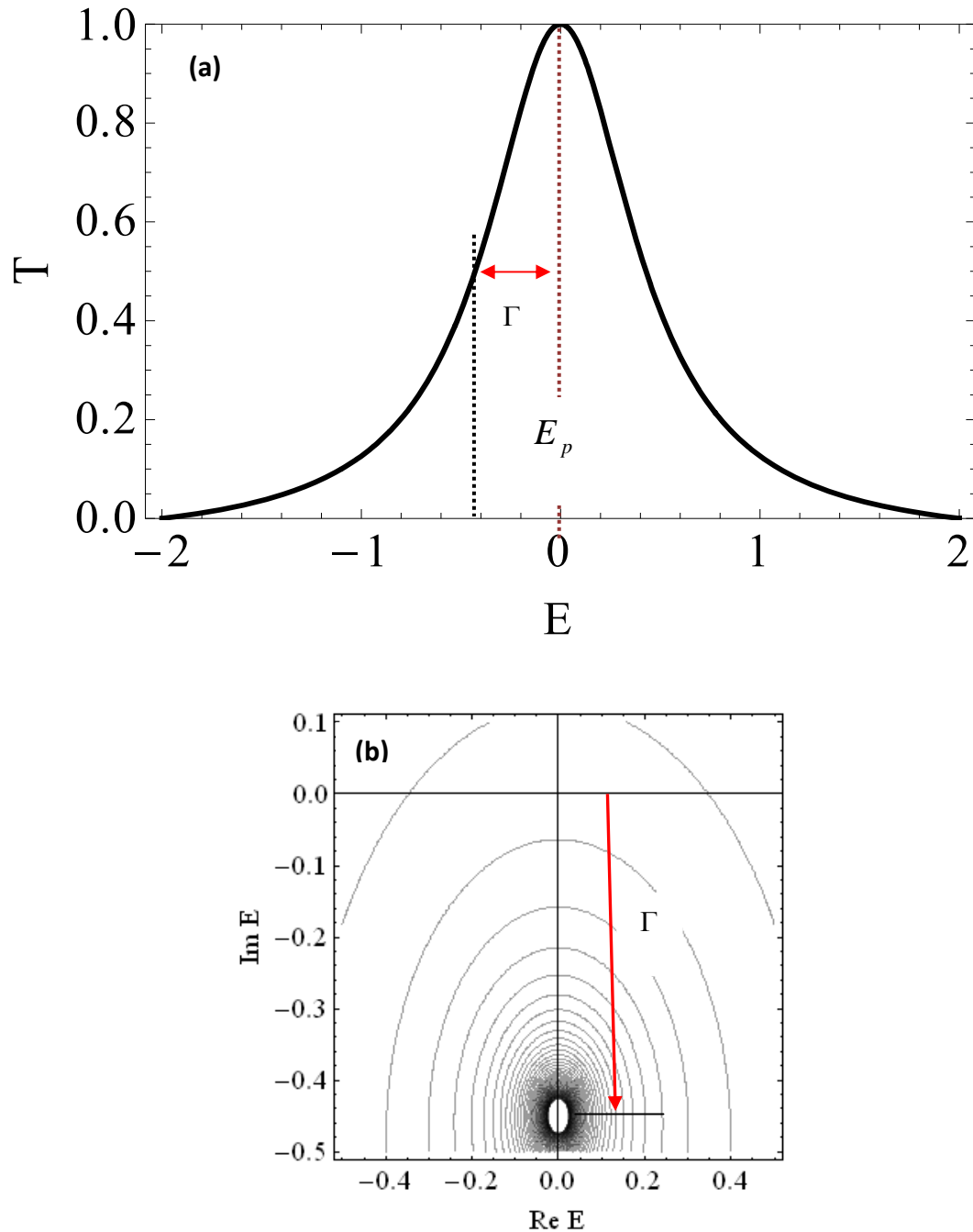


Figure 2.4 Double barrier resonant tunneling shows a typical BW resonance (Eqs. (2.6) and (2.7)). (a) Transmission probability on the real-energy axis and (b) corresponding transmission amplitude in the complex-energy plane. The BW resonance has a peak at  $E_p$ .

$$t(z) \sim \frac{(z - E_0)}{z - (E_p - i\Gamma)}, \quad (2.8)$$

which is based on a zero-pole pair in the complex-energy plane;  $E_0$  and  $(E_p - i\Gamma)$  denote the positions of the transmission zero and pole, respectively. For an asymmetrical Fano-type resonance,  $E_0$  and  $E_p$  are not the same. From Eq. (2.8), an expression for the transmission probability along the real axis is derived as [21]

$$T(E) = C \frac{(E - E_0)^2}{(E - E_p)^2 + \Gamma^2}, \quad (2.9)$$

where the normalization constant  $C = \Gamma^2 / [(E_p - E_0)^2 + \Gamma^2]$ .

Fano found, in Ref. [9], that the autoionization cross section could be exclusively parameterized by  $(q + \varepsilon)^2 / (1 + \varepsilon^2)$ , where  $\varepsilon$  is a reduced energy and  $q$  is regarded as a parameter. The two parameterized values are defined as<sup>1</sup>

$$\varepsilon = (E - E_p) / \Gamma \quad \text{and} \quad q = (E_p - E_0) / \Gamma. \quad (2.10)$$

With the parameterized expression, the transmission can be rewritten as a function of  $\varepsilon$  :

---

<sup>1</sup> Note that in his original paper  $E_{res}$ , the energy of the resonant state, was used instead of  $E_p$ . But the real part of the pole energy,  $E_p$ , corresponds to  $E_{res}$  [19].

$$T(\varepsilon) = \frac{(\varepsilon + q)^2}{(1 + q^2)(1 + \varepsilon^2)}. \quad (2.11)$$

For the  $q$  value much greater than zero, Eq. (2.11) is changed to

$$T(\varepsilon) \approx \frac{1}{\varepsilon^2 + 1} = \frac{\Gamma^2}{(E - E_p)^2 + \Gamma^2}, \quad (2.12)$$

which approximates the BW resonance in Eq. (2.7). Therefore, we could say that BW resonance is another case of the Fano resonance.

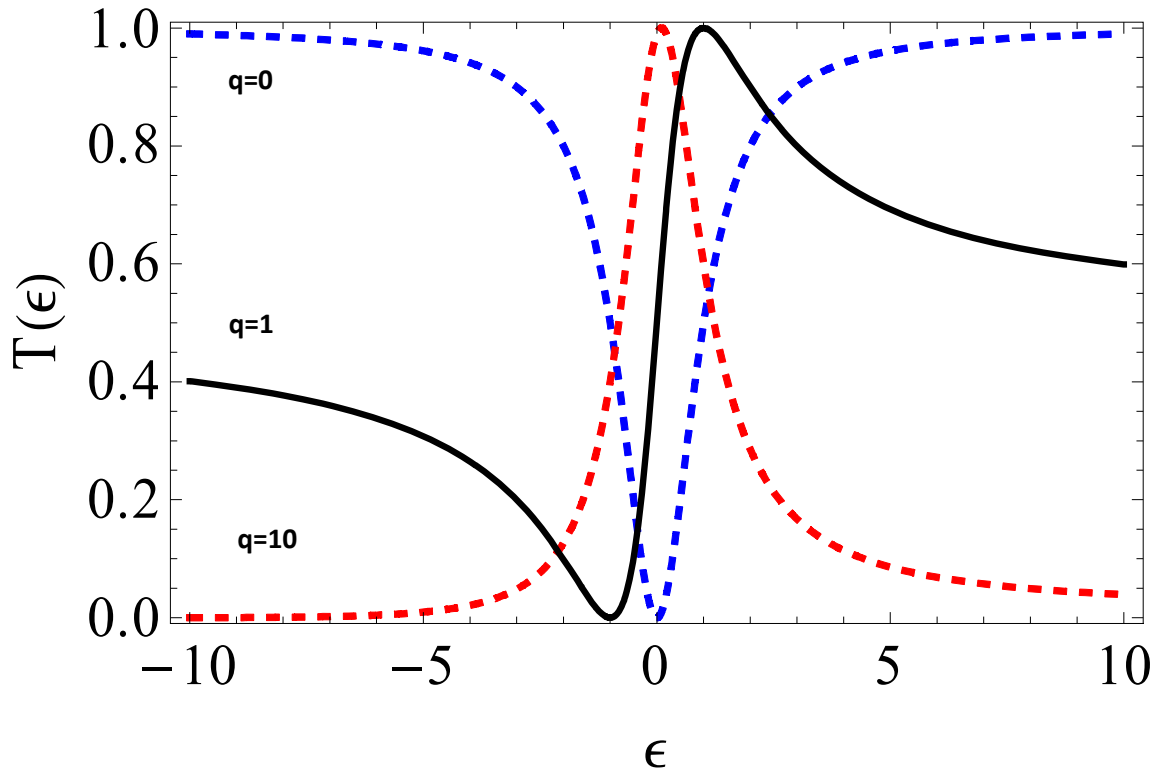


Figure 2.5 Eq. (2.13) is plotted as a function of  $\varepsilon$  when  $q$  value is varied. The blue dashed line ( $q=0$ ) is a Fano-dip type resonance while the red dashed line ( $q=10$ ) is a BW type resonance. The black solid line ( $q=1$ ) shows a typical Fano resonance.

When  $q$  approaches to zero, then

$$T(\varepsilon) \approx \frac{\varepsilon^2}{\varepsilon^2 + 1} = \frac{(E - E_p)^2}{(E - E_p)^2 + \Gamma^2}, \quad (2.13)$$

which approximates a Fano dip anti-resonance. Transmission curves for three different values of the Fano parameter  $q$  are shown in Fig. 2.5.

## CHAPTER 3: The tight-binding model

### 3.1 Introduction

For a metal in which there are nearly free conduction electrons, only weakly perturbed by the periodic potential of the ions, we explain the electron motion with the nearly-free electron model when calculating electronic levels [22]. With this method, we could study the band gap which can be explained by the standing waves at the zone boundary. However for materials which are formed from closed-shell atoms or ions, or even covalent solids, it's revealed that the free electron model seems inappropriate to explain the heat capacity at a specific temperature even though free electron theory successfully accounts for a wide range of metallic properties. Here the tight binding approximation is most useful for describing the periodic potential in which the wave functions are overlapped between the lattices.

Let us start with separated neutral atoms and watch the changes in the atomic energy levels as the charge distributions of adjacent atoms overlap when the atoms are brought together to form a crystal [23]. Suppose we have two hydrogen atoms separated by a very large distance. As the atoms are brought together, their wavefunctions overlap. We consider the two combinations  $\psi_A \pm \psi_B$  (Fig. 3.1). Each combination shares an

electron with the two protons, but an electron in the state  $\psi_A + \psi_B$  will have a somewhat lower energy than in the state  $\psi_A - \psi_B$ .

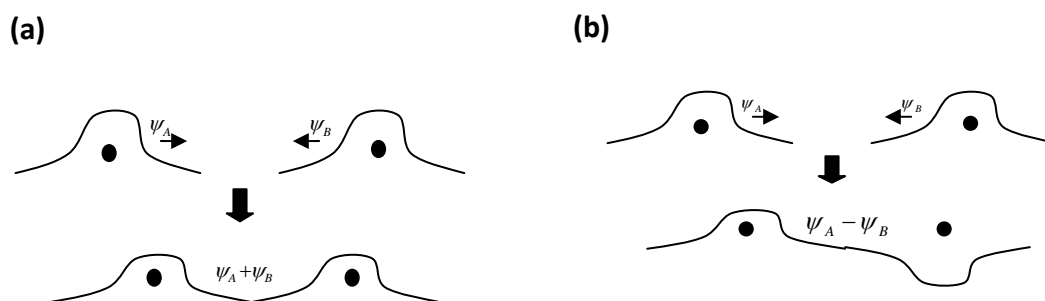


Figure 3.1 Schematic drawing of wavefunctions of electrons on two hydrogen atoms at large separation (upper). (a) Ground state wavefunction at closer separation (lower). (b) Excited state wavefunction (lower) [23].

When the atoms are separated by a large distance, there are two states, each at  $-13.6V$ , so the total energy at  $R=\infty$  is  $-27.2V$ . When the separation is reduced, there are still two states, but now at different energies. One state corresponds to the sum of the two wavefunctions and leads to a stable  $H_2$  molecule; the other state corresponds to the difference of the two wavefunctions and does not give a stable molecule. The molecular state that leads to a stable molecule is known as a bonding state, and the one that does not lead to a stable molecule is an antibonding state.

As two atoms are brought together, two separated energy levels are formed for each level of the isolated atom. For  $N$  atoms,  $N$  orbitals are formed for each orbital of the isolated atom. The tight-binding approximation, often called the LCAO (linear combination of atomic orbitals) deals with the case in which the overlap of atomic wave function is enough to require corrections to the picture of isolated atoms. The approximation is quite good for the inner electrons of atoms.

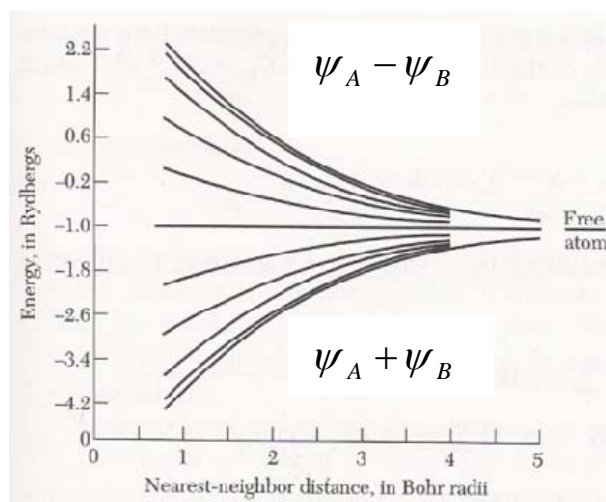


Figure 3.2 The 1s band of a ring of 20 hydrogen atoms; the one-electron energies are calculated in the tight-binding approximation with the nearest-neighbor overlap integral [23].

### 3.2 General formalism

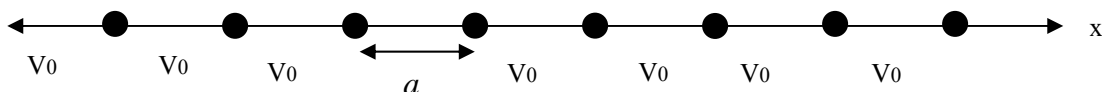


Figure 3.3 One dimensional lattice in a crystal with lattice spacing ' $a$ '. The atomic wave functions have such a short range that only nearest-neighbor terms are considered in a calculation, with overlap integral,  $V_0$ .

To begin with, we consider a simple crystal structure. An ideal crystal is constructed by the infinite repetition of the basis of atoms. In a periodic lattice, the interaction between nearest neighbors is the same over the crystal. In developing the tight-binding approximation, we assume that in the vicinity of each lattice point the full periodic crystal Hamiltonian,  $H$ , can be approximated by the Hamiltonian,  $H_{at}$ , of a single atom located at the lattice point. We also assume that the bound levels of the atomic Hamiltonian are well localized:

$$H_{at} \Psi_n = E_n \Psi_n . \quad (3.1)$$

The wave function of the electrons in the periodic lattice can be expressed as the sum of the linear combination of separable solutions :

$$\Psi(x,t) = \sum_n c_n \psi_n(x,t) = \sum_n c_n \varphi_n(x) \phi_n(t) . \quad (3.2)$$

It is very straightforward to write down the general linear combination of this solution for a time-independent Schrödinger equation:

$$\Psi(x,0) = \sum_n c_n \varphi_n(x) . \quad (3.3)$$

In a periodic lattice, according to Bloch's theorem, the wavefunction becomes

$$\Psi_n(x) = \psi_0(x - na) , \quad (3.4)$$

where  $a$  is a lattice constant, which is the distance between nearest-neighbors. In the same manner, we choose to view the periodic potential as a superposition of potential barriers  $v(x)$  of width  $a$ , centered at the points  $x = \pm na$  (Fig. 3.3):

$$U(x) = \sum_n v(x - na), \quad (3.5)$$

where  $U(x)$  is the sum of potential over the all lattices. Only considering nearest neighbors, the wave function at site ' $n$ ' is expressed as a combination of the nearest neighbors,

$$\Psi_n = c_{n-1}\varphi_{n-1} + c_n\varphi_n + c_{n+1}\varphi_{n+1} . \quad (3.6)$$

The total Hamiltonian in the lattice is given in operator form by

$$\hat{H}(x, \hat{p}) = \frac{\hat{p}^2}{2m} + \sum_n v(x - na) . \quad (3.7)$$

In periodic lattice structures, the potential is the same for each lattice site with finite coupling between sites. Assuming that atoms only interact with nearest neighbors, the total Hamiltonian reduces to

$$H = \frac{\hat{p}^2}{2m} + v_{n-1} + v_n + v_{n+1} . \quad (3.8)$$

Substituting Eq. (3.8) into the Schrödinger equation,  $H\Psi_n = E\Psi_n$ , we have this equation:

$$\left( \frac{\hat{p}^2}{2m} + v_{n-1} + v_n + v_{n+1} \right) (c_{n-1}\varphi_{n-1} + c_n\varphi_n + c_{n+1}\varphi_{n+1}) = E(c_{n-1}\varphi_{n-1} + c_n\varphi_n + c_{n+1}\varphi_{n+1}). \quad (3.9)$$

Each individual site function satisfies

$$\left( \frac{\hat{p}^2}{2m} + v_n \right) c_n \varphi_n = \varepsilon_n c_n \varphi_n, \quad (3.10)$$

which, when used in Eq.(3.9), leads us to

$$\begin{aligned} \varepsilon_{n-1}c_{n-1}\varphi_{n-1} + \varepsilon_n c_n \varphi_n + \varepsilon_{n+1}c_{n+1}\varphi_{n+1} + c_n v_{n-1}\varphi_n + c_{n+1}v_{n-1}\varphi_{n+1} + c_{n-1}v_n\varphi_{n-1} + \\ c_{n+1}v_n\varphi_{n+1} + c_{n-1}v_{n+1}\varphi_{n-1} + c_n v_{n+1}\varphi_n = E(c_{n-1}\varphi_{n-1} + c_n\varphi_n + c_{n+1}\varphi_{n+1}) \end{aligned} \quad (3.11)$$

Notice that we could have dropped terms for which the overlap integral involves a wave function which is not a nearest-neighbor to the potential. The wave function is so localized that it hardly affects other sites, except nearest neighbors. Some product terms may be ignored; for example, the  $(n-1)$ th potential is not overlapped with the  $(n+1)$ th wave function. In the same manner, the potential of the  $(n+1)$ th site doesn't affect the  $(n-1)$ th wave function. So their product is neglected:  $v_{n-1}\varphi_{n+1} \approx 0$  and  $v_{n+1}\varphi_{n-1} \approx 0$ . Now, the  $\varphi_n(x)$  are orthonormal, meaning  $\int \varphi_n \varphi_m dx = \delta_{nm}(x)$ . This allows us to multiply Eq. (3.11)

by  $\varphi_n$  on both sides and integrate over the lattice to obtain

$$\varepsilon_n c_n + c_n (v_{n-1})_{n,n} + c_{n-1} (v_n)_{n,n-1} + c_{n+1} (v_n)_{n,n+1} + c_n (v_{n+1})_{n,n} = E c_n,$$

which can be rearranged in terms of  $c_n$ :

$$c_n(\varepsilon_n + (v_{n-1})_{n,n} + (v_{n+1})_{n,n}) + c_{n-1}(v_n)_{n,n-1} + c_{n+1}(v_n)_{n,n+1} = Ec_n . \quad (3.12)$$

Eq. (3. 12) can be simplified to

$$c_n \bar{\varepsilon}_n + c_{n-1}(v_n)_{n,n-1} + c_{n+1}(v_n)_{n,n+1} = Ec_n , \quad (3.13)$$

where  $\bar{\varepsilon}_n = \varepsilon_n + (v_{n-1})_{n,n} + (v_{n+1})_{n,n}$  . If we define  $c_n \equiv \psi_n$ , Eq. (3.13) can be re-written as

$$-[V_{n,n-1}\psi_{n-1} + V_{n,n+1}\psi_{n+1}] + \bar{\varepsilon}_n\psi_n = E\psi_n . \quad (3.14)$$

This is the Schrödinger equation in the tight-binding approximation in a 1-dimensional system. For a two-dimensional system, the term in a square bracket can be extended to include multiple “nearest-neighbors” of site  $n$  .

### 3.3 Dispersion relation

According to the Bloch theorem, we propose a periodic solution in  $k$ -space of the form

$$\psi_n = Ae^{i\theta n} \quad (\theta = ka) .$$

Substituting this into Eq. (3.14), we have

$$-(V_{n,n-1}Ae^{i\theta(n-1)} + V_{n,n+1}Ae^{i\theta(n+1)}) + \bar{\varepsilon}_n Ae^{i\theta n} = EAe^{i\theta n} .$$

Canceling 'A' on both sides and re-arranging the equation, we obtain

$$E = -(V_{n,n-1}e^{-i\theta} + V_{n,n+1}e^{i\theta}) + \bar{\varepsilon}_n$$

Assuming that the lattice is uniform and periodic so that the overlap coupling is fixed at  $V_0$  in the one-dimensional lattice, we obtain the dispersion relation derived for a 1-dimensional uniform lattice:

$$\boxed{E = -2V_0 \cos\theta + \bar{\varepsilon}_n} \quad (3.15)$$

(Notice that  $e^{-i\theta} = \cos\theta - i\sin\theta$ ,  $e^{i\theta} = \cos\theta + i\sin\theta$ ).

### 3.4 Double barrier resonance tunneling (DBRT) in a 1D periodic lattice

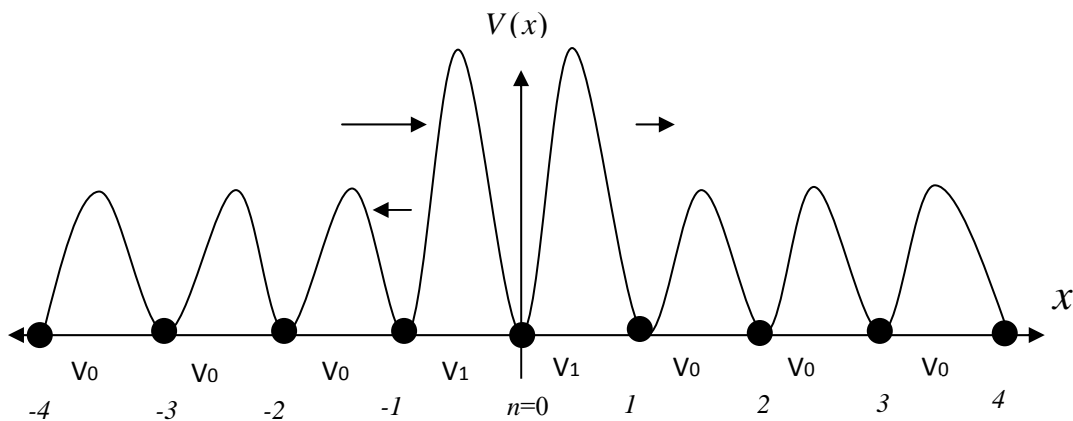


Figure 3.4 The curve depicts a periodic potential structure drawn along a line of atomic sites. Two potentials around the origin are bigger than the others making a double barrier resonance structure.

For a 1D lattice, the wave function is given by

$$\psi_n = e^{i\theta n} + r e^{-i\theta n} \quad (n < 0) \quad (3.16)$$

$$\psi_n = t e^{i\theta n} \quad (n > 0) ,$$

where ‘ $r$ ’ is the reflection amplitude and ‘ $t$ ’ is the transmission amplitude. Notice that the overlapped wave function (at  $n = 0$ ) is not given, but is one of the unknowns. Using Eq. (3.14), we have the following equations:

For ( $n = -1$ ) , Eq. (3.14) becomes

$$-[V_0\psi_{-2} + V_1\psi_0] + \bar{\varepsilon}_{-1}\psi_{-1} = E\psi_{-1}. \quad (3.17)$$

Applying appropriate wavefunctions to Eq. (3.17) and re-arranging it, we have

$$-V_1\psi_0 - (V_0 e^{2i\theta} - \bar{\varepsilon}_{-1} e^{i\theta} + E e^{i\theta})r = -V_0. \quad (3.18)$$

The dispersion relation, Eq. (3.15), can be rewritten as a combination of exponential forms:

$$E = -2V_0 \left( \frac{e^{i\theta} + e^{-i\theta}}{2} \right) + \varepsilon_n .$$

Multiplying both sides by  $e^{i\theta}$  leads to

$$E e^{i\theta} = -V_0 e^{2i\theta} - V_0 + \varepsilon_n e^{i\theta} . \quad (3.19)$$

Assuming that in a uniform lattice the site energy  $\varepsilon_n$  is the same for any value of 'n' except at the origin, we drop the subscript 'n' in Eq. (3.19) to obtain

$$V_0 = -(V_0 e^{2i\theta} - \varepsilon e^{i\theta} + E e^{i\theta}).$$

With this, Eq. (3.18) is simplified to

$$-V_1 \psi_0 + V_0 r = -V_0. \quad (3.20)$$

For ( $n = 0$ ), again Eq. (3.14) is changed to

$$-V_1 \psi_{-1} - V_1 \psi_1 + (\varepsilon_0 - E) \psi_0 = 0,$$

and doing the exact same procedure as for  $n = -1$ , we have

$$-r V_1 e^{i\theta} - V_1 e^{i\theta} t + (\bar{\varepsilon}_0 - E) \psi_0 = V_1 e^{-i\theta}. \quad (3.21)$$

For ( $n = 1$ ), we have

$$\begin{aligned} -V_1 \psi_0 - V_0 \psi_2 + (\varepsilon_0 - E) \psi_1 &= 0, \\ -V_1 \psi_0 + V_0 t &= 0. \end{aligned} \quad (3.22)$$

Assuming that only nearest neighbor lattices interact with each other, we obtain three equations with three unknowns. Now we are ready to solve the equations in terms of  $r$ ,  $t$  and  $\psi_0$ .

Combining Eq. (3.22) and Eq. (3.20), we have

$$V_0 r - V_0 t = -V_0,$$

where  $V_0$  terms can be cancelled on both sides:

$$r = t - 1. \quad (3.23)$$

Substituting Eq. (3.23) into Eq. (3.21) to drop the reflection amplitude ‘  $r$  ’ give

$$-2V_1 e^{i\theta} t = V_1 (e^{-i\theta} - e^{i\theta}) + (E - \varepsilon_0) \psi_0 .$$

From Eq. (3.22),  $\psi_0 = \frac{V_0}{V_1} t$ , so the previous expression can be written as

$$[(E - \varepsilon_0)V_0 - 2V_1^2 e^{i\theta}] t = V_1^2 (e^{-i\theta} - e^{i\theta}) .$$

Finally, the transmission amplitude  $t(E)$  is

$$t(E) = \frac{2iV_1^2 \text{Sin}\theta}{2V_1^2 e^{i\theta} + (E - \varepsilon_0)V_0} . \quad (3.24)$$

From Eq. (3.23) we can also find the reflection amplitude  $r(E)$ :

$$r(E) = \frac{2iV_1^2 \text{Sin}\theta}{2V_1^2 e^{i\theta} + (E - \varepsilon_0)V_0} - 1 . \quad (3.25)$$

We have found the transmission and reflection amplitudes as a function of the incoming electron energy, with other variables as parameters. Of course, the sum of the two probabilities ( $|t|^2 + |r|^2$ ) should be 1 and it means (see Fig. 3.5, the solid red line):

$T + R = 1$  .  $T = |t|^2$  is the transmission coefficient and  $R = |r|^2$  denotes the reflection coefficient. We are interested in studying the transmission amplitude, since we focus our research on quantum tunneling. Figure 3.5 shows the results for a double barrier resonant tunneling structure with a well-confined quasi-bound state.

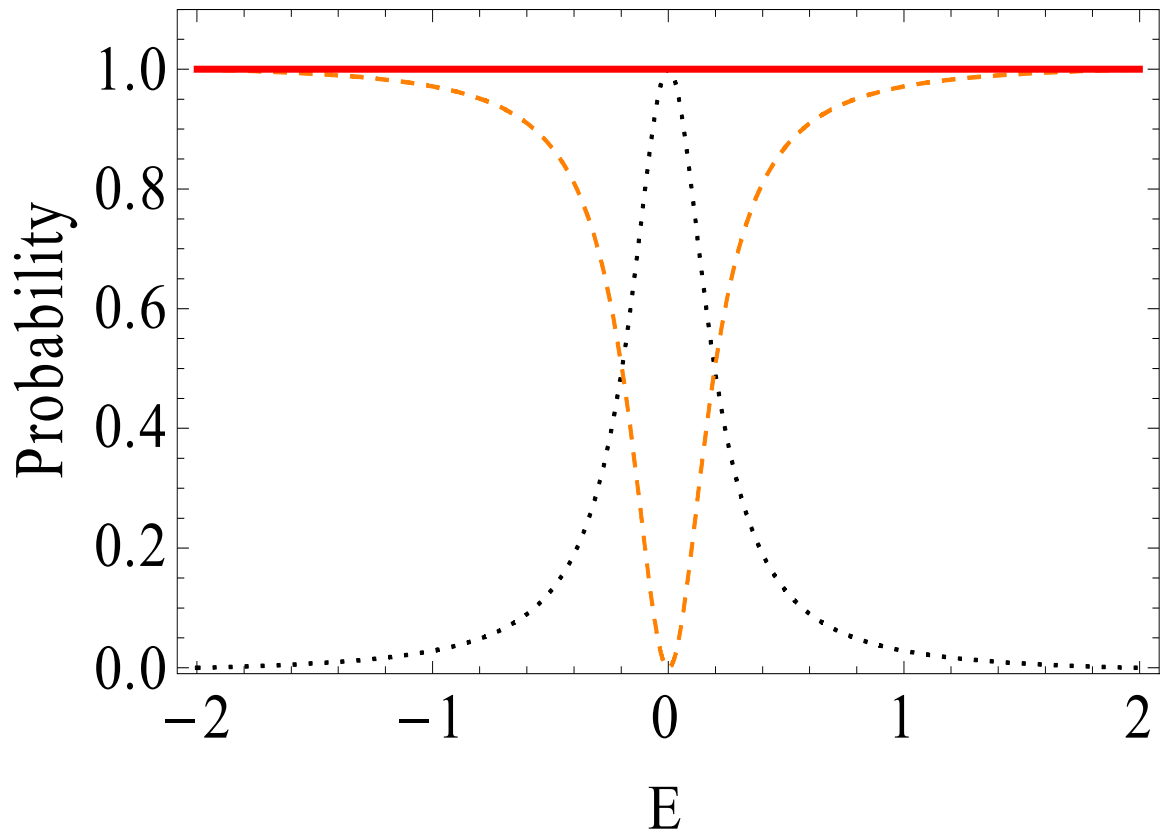


Figure 3.5 Transmission probability  $|t(E)|^2$  (black dotted line) plus the reflection coefficient  $|r(E)|^2$  (dashed orange line) is always 1 (solid red line) as expected. The black dotted symmetric line shows the BW resonance for double barrier resonant tunneling. This is plotted for  $\bar{\epsilon}_0 = 0$ ,  $V_0 = 1$ , and  $V_1 = 0.3$ .

### 3.5 Discrete energy state

Assuming the bound-state electron can be controlled experimentally, we predict the transmission resonances in a one dimensional DBRT structure. Figure 3.6 shows that the resonance peaks are dependent on the quasi-bound state. To help see this trend more easily, we set  $V_1$  symmetrically. The dotted orange line in Fig. 3.6(a) is for  $\bar{\varepsilon}_0 = -0.5$  while the solid line results from  $\bar{\varepsilon}_0 = 0.5$ . In each case the peaks are positioned dependent upon the confined energy state. These pictures are well understood, as other articles have shown in Ref. [17-21] that the incident energy of the electrons is resonant with one of the quasi-bound energy levels of the structure. In our approach, the number of resonances corresponds to the number of bound states.

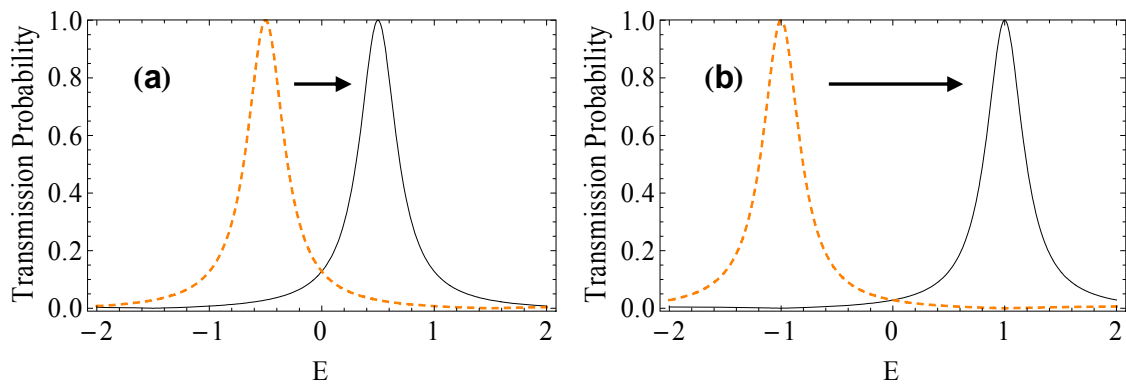


Figure 3.6 The transmission coefficient of a double barrier structure plotted as a function of incident energy  $E$ . Resonance poles depend on the quasi-bound state energy  $\bar{\varepsilon}_0$  of the symmetric double barrier. In (a),  $\bar{\varepsilon}_0 = -0.5$  (dotted line)  $\rightarrow$   $0.5$  (solid line). In (b)  $\bar{\varepsilon}_0 = -1$  (dotted line)  $\rightarrow$   $1$  (solid line),  $V_1 = 0.3$ , and  $V_0 = 1$ .

### 3.6 The nearest neighbor coupling effect

Now one can wonder how well we could confine the quasi-bound state electron in a double barrier. We predict that the nearest neighbor coupling is a parameter to decide the strength of confinement of a quasi-bound state. Notice that in our set-up (Fig. 3.3) the nearest neighbor couplings are the same over the periodic lattice structure, except at the origin. In other words,  $V_0$  is fixed at  $V_0=1$  and  $V_1$  is varied to make a barrier to confine a quasi-bound state electron. Figure 3.7 shows that the confinement is weaker as  $V_1$  is larger. So we can find this relationship between the barrier height,  $U$ , and the nearest neighbor coupling:

$$\text{barrier height } U \propto \frac{1}{V_1} . \quad (3.26)$$

The lifetime of quasi-bound states becomes long with weak lead-dot couplings because the infinitely narrowing of a resonance in the transmission coefficient implies that an electron is completely localized in the system [7, 11, 18, 19]<sup>1</sup>. In Fig. 3.7(b), the transmission probability becomes unity for  $V_1=1$  (solid red line) in which case the double barrier resonant state no longer exist. This occurs when the nearest neighbor coupling is

---

<sup>1</sup>For resonant tunneling in a double-barrier GaAs/AlGaAs hetero structure, it is known that the Lorentzian half-width of the transmission peak,  $\Delta E$ , is related to the combined lifetime  $\tau$  for tunneling out of the well region through either of the two enclosing barriers by

$$\hbar / \tau = 2\Delta E .$$

the same as other coupling strengths. In this case there is no quasi-bound state confined, and the transmission is 100% across the energy range.

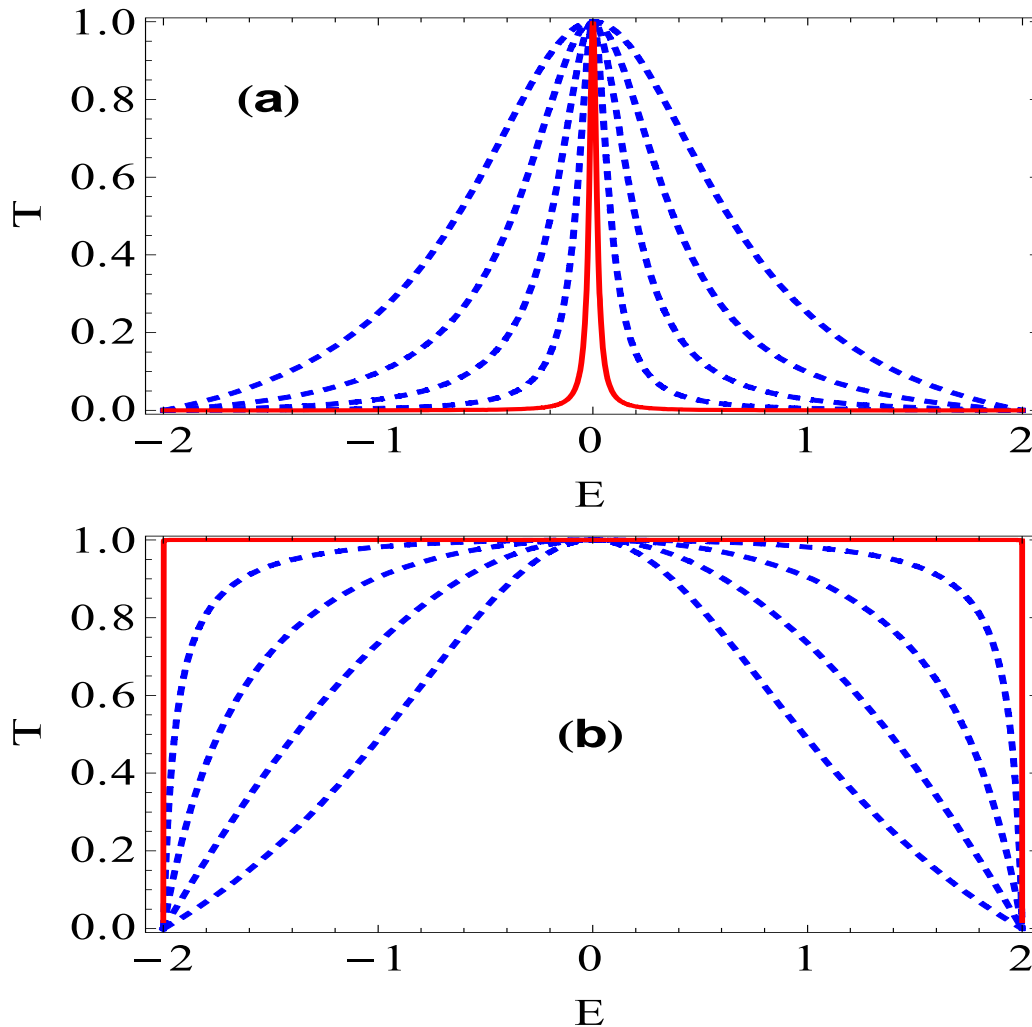


Figure 3.7 Transmission probability of a double barrier structure as a function of incident energy  $E$ . (a) The resonance gets wider as the nearest neighbor coupling  $V_1$  increases from the solid red line to outer - 0.1 (center), 0.2, 0.3, 0.4, and 0.5 (outer line). (b) The solid red line indicates  $V_1 = 1.0$ .  $V_1$  increases from the center to outer (solid red line) - 0.6 (center), 0.7, 0.8, 0.9, 1 (solid red line). When  $V_1$  is equal to  $V_0$ , the transmission is '1' for all the regions of incident energy.

## Chapter 4: Electron transport in a double quantum dot

### 4.1 Introduction

We studied resonance phenomena of an electron in a simple one-dimensional double barrier in the previous chapter. With the tight-binding model, we found the transmission probability and studied the confinement of quasi-bound states. Now we are ready to study the electron transport by defining the QDs within a 2DEG at the interface of an AlGaAs/GaAs heterostructure.

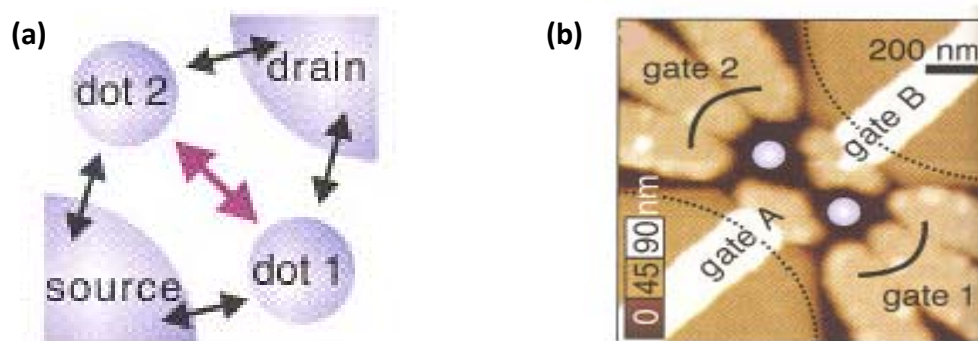


Figure 4.1 (a) Experimental layout from A. W. Hollietner *et al* [24]. Two QDs are formed within a 2DEG 90nm below the surface of an AlGaAs/GaAs heterostructure. Electrons tunnel via both dots from source to drain (black arrows). Coupling between the two dots (red arrow) is tuned by voltages applied to gate **A** and **B**. (b) AFM picture of the sample. The heights are color coded as indicated on the lower left. To define two QDs, negative voltages are applied to gates **A**, **B**, **1**, and **2**. Both QDs are equally connected to drain and source contacts.

Figure 4.1(a) is the experimental layout by Hollietner *et al.* [24] in which the exchange of electrons between both dots is detected by measuring the system's

conductance through the cotunneling mechanism. The overlap of the dot wave functions can be tuned by the tunneling barrier, set by voltages on gates **A** and **B** in Fig.4.1 (b).

In order to complete the setup of Fig. 4.1(a), the source and drain contact regions of both dots (dashed lines) are patterned by an additional layer which is colored beige in Fig. 4.1(b). This layer prevents depletion of the electron gas below gates **A** and **B**, and electrons eventually tunnel through dot 1 and dot 2 [7, 24].

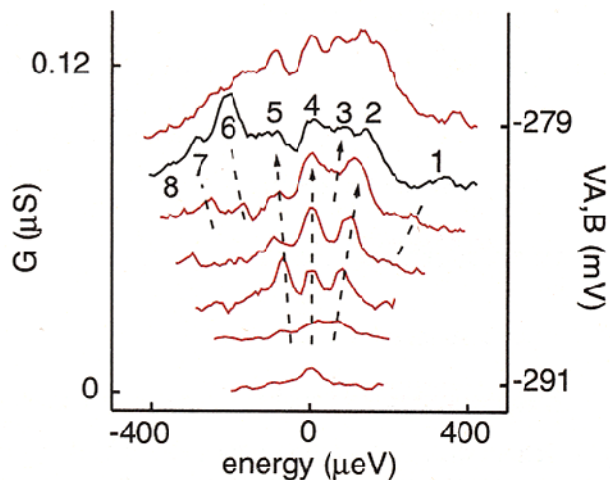


Figure 4.2 Conductance plots obtained from a double quantum dot at 815mK traced by cotunneling of the two binding electrons. The resonances 1 through 8 are picked at  $V_2 = -430\text{mV}$  when  $V_1$  is varied from  $-450\text{mV}$  to  $-460\text{mV}$ . Increasing the negative voltages applied to gate A and B from  $-279\text{mV}$  to  $-291\text{mV}$  raised the inter-dot tunneling barrier, which in turn suppresses all but one of the resonances. The data are presented with an offset for better visibility [24].

In Ref. [24], Holleitner *et al.* demonstrates how the molecular quantum state of coupled semiconductor QDs are probed and manipulated in transport experiments. Figure 4.2 is one of their results showing the conductance plots for a molecular state of QDs in the regime of thermally broadened resonances [25]. They also show in Fig. 4.2 that raising the inter-dot barrier reduces the number of resonances to one. In chapter 5, using

our theoretical model, we show how the number of resonances is affected by the magnitude of inter-dot coupling.

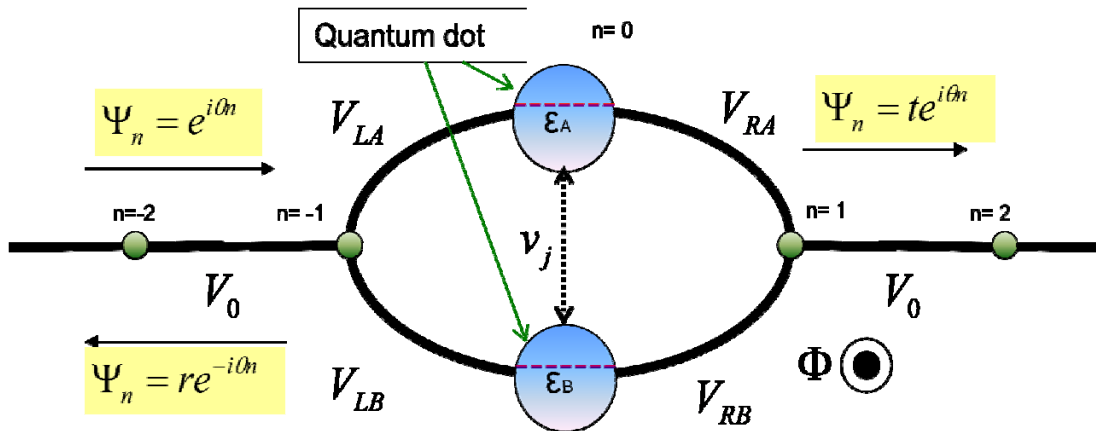


Figure 4.3 A schematic of Aharonov-Bohm ring. Two QDs are weakly coupled with  $v_j$ . A magnetic field perpendicular to the ring is applied.

Based on the setup in Fig. 4.1, we trace the transmission amplitude in a balanced AB ring ( $V_{LA} = V_{RA} = V_{LB} = V_{RB} = V_1$ ) with identical QDs in each arm (Fig. 4.3) by solving the Schrödinger equation in the tight-binding approximation. In this chapter, the transmission coefficient is plotted not only as a function of incident energy but also as a function of magnetic flux. Our results confirm that the AB ring's conductance oscillates when a variable magnetic field penetrates its inner core, with a periodicity of the flux quantum  $h/e$ . We continue to focus our attention on the position of the transmission zero and pole, denoted by  $E_0$  and  $E_p$ , respectively. We predict the transmission zero as a function of incident energy numerically. Notice that in our model (Fig. 4.3) there is one

quasi bound state in each dot ( $\varepsilon_A$  and  $\varepsilon_B$ ) which is coupled to the other dot. Coupling between dots is controlled by the inter-dot coupling parameter  $v_j$ . The case with two energy states in each dot will be studied in chapter 5. We use *Wolfram Mathematica 6.0* to generate and investigate the transmission plots.

## 4.2 Formalism

The solution of the wave function in the tight-binding approximation as the incident particle is passing through the ring is given as

$$\psi_n = e^{i\theta n} + re^{-i\theta n} \quad (n < 0), \quad (4.1)$$

$$\psi_n = te^{i\theta n} \quad (n \geq 1),$$

where  $\theta$  is  $ka$ <sup>1</sup>. Again, we rewrite the Schrödinger equation in the tight-binding approximation as

$$-[V_{n,n-1}\psi_{n-1} + V_{n,n+1}\psi_{n+1}] + \varepsilon_n\psi_n = E\psi_n. \quad (4.2)$$

Now, we substitute Eq. (4.1) into Eq. (4.2) for the cases of  $n = -1, 0, 1$  which correspond to the nearest-neighbor lattices. In our calculations, the site energies  $\varepsilon_n$  are set to zero for all sites except for the QDs at  $n=0$  which have site energies  $\varepsilon_A$  and  $\varepsilon_B$ , respectively.

---

<sup>1</sup> 'a' is the lattice constant.

Phase factors in two paths due to the magnetic flux are considered. We choose a symmetric gauge such that  $V_{LA} = V_{LB} = V_{RA} = V_{RB} = V_1 \exp(\pm i\varphi/4)$  [26], where the minus signs are applied when the electron moves in the clockwise direction. The electrons moving from  $n = -1$  to  $n = 0$  (dot A) travel in the clockwise direction so that the minus sign is appropriate, otherwise, the plus signs are applied. Notice that the inter-dot coupling is denoted by  $v_j$  which is controlled experimentally by gates **A** and **B** (Fig. 4.1). In chapter 3, the total phase difference between two particles divided by two paths enclosing flux  $\Phi$  was given as  $2\pi\Phi/\Phi_0$ . Figure 4.4 illustrates how the phase factors are applied. Let  $\varphi$  be the phase for each site, giving the total phase difference as the sum of each phase,

$$\text{Total phase difference} = \left| -\frac{\varphi}{4} \right| + \left| -\frac{\varphi}{4} \right| + \left| \frac{\varphi}{4} \right| + \left| \frac{\varphi}{4} \right| = \varphi \quad , \quad (4.3)$$

which must be equal to Eq. (2.4):

$$\varphi = 2\pi \frac{\Phi}{\Phi_0} \quad . \quad (4.4)$$

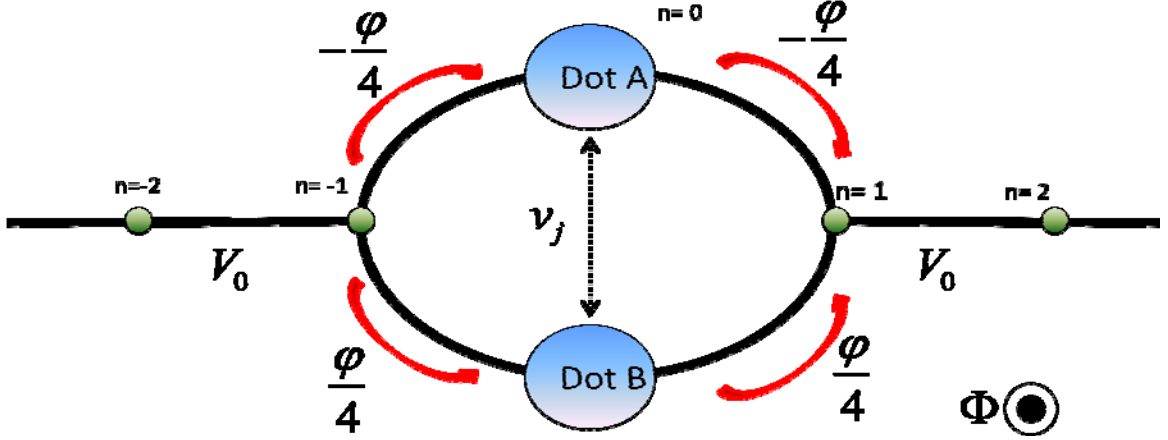


Figure 4.4 Phase difference from the lattice point at  $n=-1$  to another dot at  $n=1$  is  $\varphi$  in an AB ring. Minus signs are for the clockwise traversals and plus signs for counter-clockwise motion. The total phase difference is the sum of the absolute values of each phase factor (Eq. (4.3)).

After somewhat lengthy derivation<sup>1</sup>, we have the transmission amplitude:

$$t(E, \varphi) = \frac{-(e^{2i\theta} - 1)V_1^2 \{E - 2e^{2i\theta}v_j - \varepsilon_A + e^{4i\theta}(E - \varepsilon_B)\}}{e^{i(3\theta - 2\varphi)}V_1^4 + e^{3i(\theta + 2\varphi)}V_1^4 + 2e^{i\theta}V_1^2v_j + 2e^{2i(\theta + 2\varphi)}V_1^2v_j + e^{i(\theta + 2\varphi)}\{-2e^{2i\theta}V_1^4 + v_j^2 - (E - \varepsilon_A)(E - \varepsilon_B) - 2e^{i\theta}V_1^2(2E - \varepsilon_A - \varepsilon_B)\}} \quad (4.5)$$

The reflection amplitude is

$$r(E, \varphi) = \frac{e^{4i\theta}[E^2 + 2V_1^4 - v_j^2 + \varepsilon_A\varepsilon_B - E(\varepsilon_A + \varepsilon_B) - 2V_1^2\{\cos\theta(-2E + \varepsilon_A + \varepsilon_B + 2v_j \cos 2\varphi) + V_1^2 \cos 4\varphi\}]}{e^{2i\theta}(e^{4i\theta} - 1)^2V_1^4 + e^{4i\theta}\{v_j^2 - (E - \varepsilon_A)(E - \varepsilon_B) + 2e^{i(\theta + 4\varphi)}V_1^2(-2E + \varepsilon_A + \varepsilon_B + 2v_j \cos 2\varphi)\}} \quad (4.6)$$

Transmission and reflection coefficients for specific parameters ( $V_1 = 0.3$ ,  $\varepsilon_A = 0.5$ ,  $\varepsilon_B = -0.5$ ,  $v_j = 0$ , and  $\varphi = 0$ ) are plotted as a function of the incident

<sup>1</sup> The calculations to find the 't' and 'r' are referred to Appendix A.

energy in Fig. 4.5, in which each quasi-bound state has its own resonance for the bonding and antibonding states if we treat the coupled QDs as molecular states.

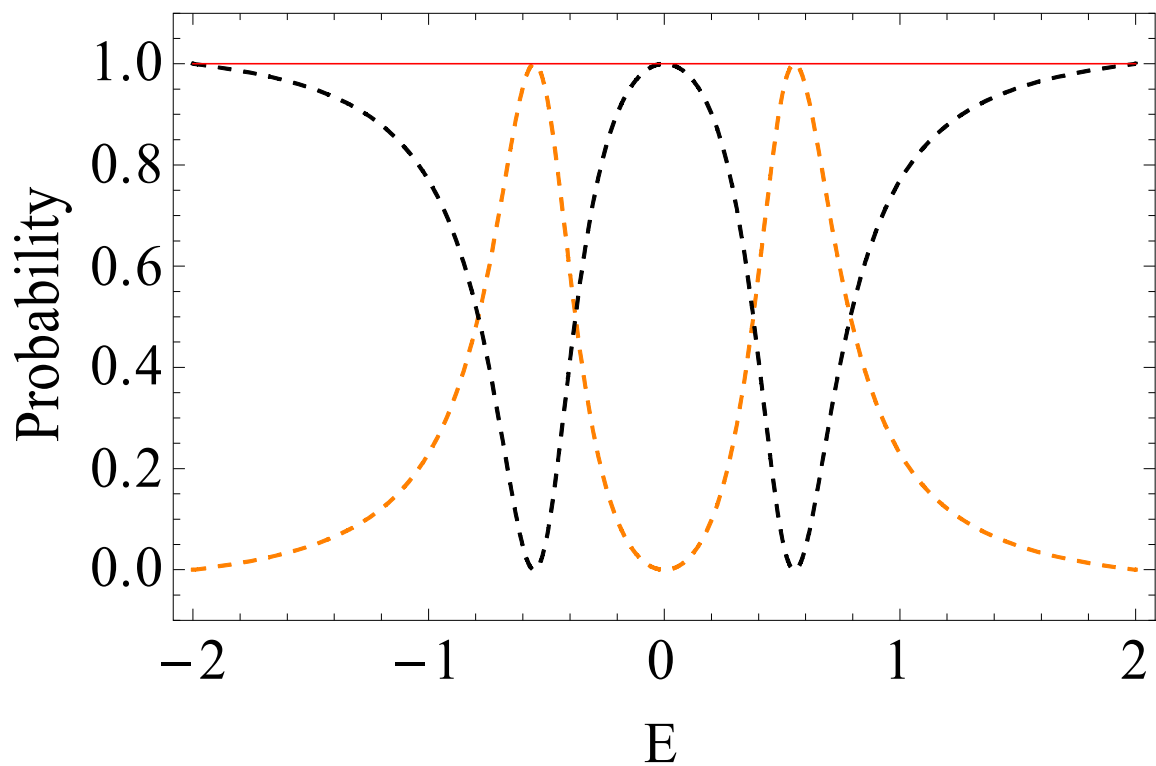


Figure 4.5 Transmission coefficient (dashed orange) plus reflection coefficient (dashed black) is always '1' (solid orange):  $T + R = 1$ . This is plotted at  $V_1 = 0.3$ ,  $\varepsilon_A = 0.5$ ,  $\varepsilon_B = -0.5$ ,  $v_j = 0$  and  $\varphi = 0$  which means there is no dot-dot interaction and no magnetic flux through the AB ring.

### 4.3 Aharonov-Bohm oscillations

Transport measurements through multiply connected geometries containing a quantum dot revealed oscillations for the conductance as a function of magnetic flux, i.e., Aharonov-Bohm oscillations. In Ref. [7], AB oscillations are observed as magnetic-flux-dependent oscillations of the electric current between source and drain (Fig. 4.6(b)) in which an electron moves from gate 1 to gate 2 via two QDs. Since electric resistance is inversely proportional to the conductance, measuring the current could account for the conductance oscillations.

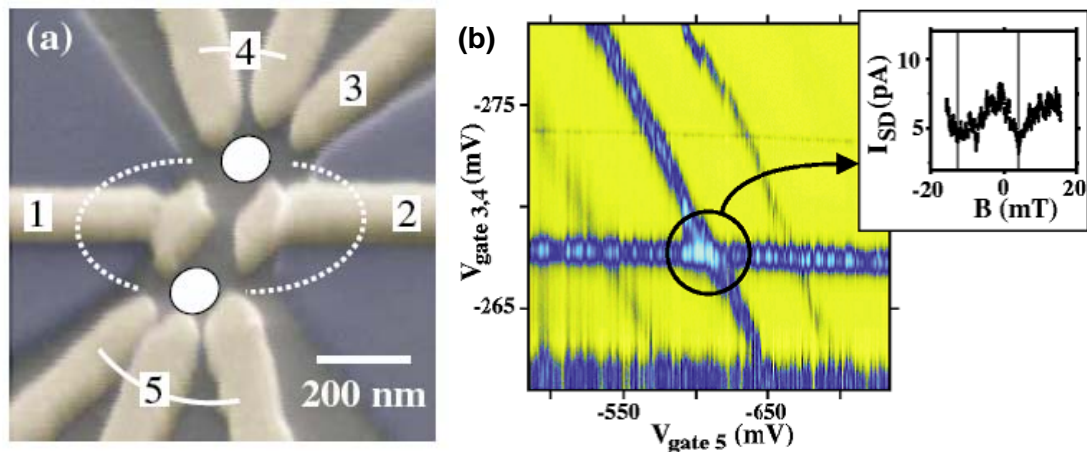


Figure 4.6 (a) The same experimental setup as in Fig. 4.1(b) by Holleitner *et al.* [7]. Gates 3,4 (above) correspond to gate 2 in Fig. 4.1(b). Gate 5 is matched with gate 1 in Fig. 4.1(b). The circles indicate the two quantum dots within the 2DEG (b) The device operates as an AB interferometer. If a magnetic field is applied perpendicular to the QDs, the amplitude of the source-drain current (gate 1 and 2) at the crossing points produces oscillations periodic with the magnetic field (inset) [7].

In our model (Fig. 4.4) we plot the oscillations of the transmission as a function of magnetic flux,  $T(\varphi)$ , for fixed level positions  $\varepsilon_A$  and  $\varepsilon_B$ , and fixed electron energy  $E$ . Figure 4.7 shows the AB oscillations for different incoming energy values. These features confirm that the oscillations have a periodicity of  $\Phi_0$ , corresponding to the flux quantum ( $h/e$ ), as we can see that it takes a change of  $\Phi/\Phi_0 = 1$  to go from peak to peak or minimum to minimum. Notice that the phase of the tunneling resonance of Fig. 4.7(a) is different from Fig. 4.7(b).

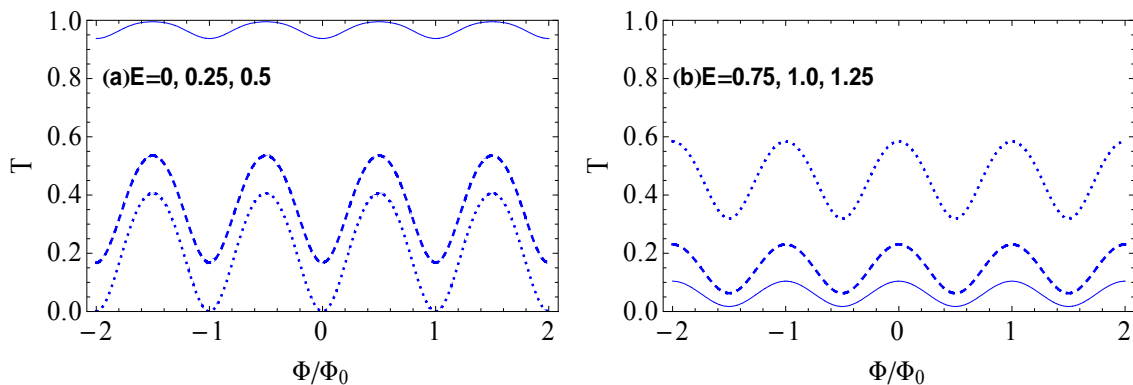


Figure 4.7 Transmission probability as a function of the magnetic flux for fixed incoming electron energies. (a)  $E=0$  (dotted), 0.25 (dashed), 0.5 (solid) and (b)  $E=0.75$  (dotted), 1.0 (dashed), 1.25 (solid line) for  $\nu_j=0$ ,  $\varepsilon_A = 0.5$ ,  $\varepsilon_B = -0.5$ , and  $\nu_1=0.3$ .

We found a very special case shown in Fig. 4.7(a). Notice that the suppressed transmission at integer value of  $\Phi/\Phi_0$  is observed only when the incoming energy is zero ( $E=0$ ) while the others are always above  $T=0$ . We find that this level ( $E=0$ ) is the average of the two dot energies ( $\varepsilon_A = 0.5$  and  $\varepsilon_B = -0.5$ ). In other words,

$E = (\varepsilon_A + \varepsilon_B)/2 = (0.5 - 0.5)/2 = 0$ . It tells us that the suppressed transmission is observed when the incoming energy approaches around the average of the two dot energy levels at every integer value of  $\Phi / \Phi_0$ . It is exactly same as in Ref. [3, 26], in which they use the notation  $\bar{\varepsilon} = (\varepsilon_A + \varepsilon_B)/2$ . We generated additional data to confirm this result. Figure 4.8(a) to (d) shows the oscillations of the transmission with a zero at every integer of  $\Phi / \Phi_0$  for various values of site energies and incident energy.

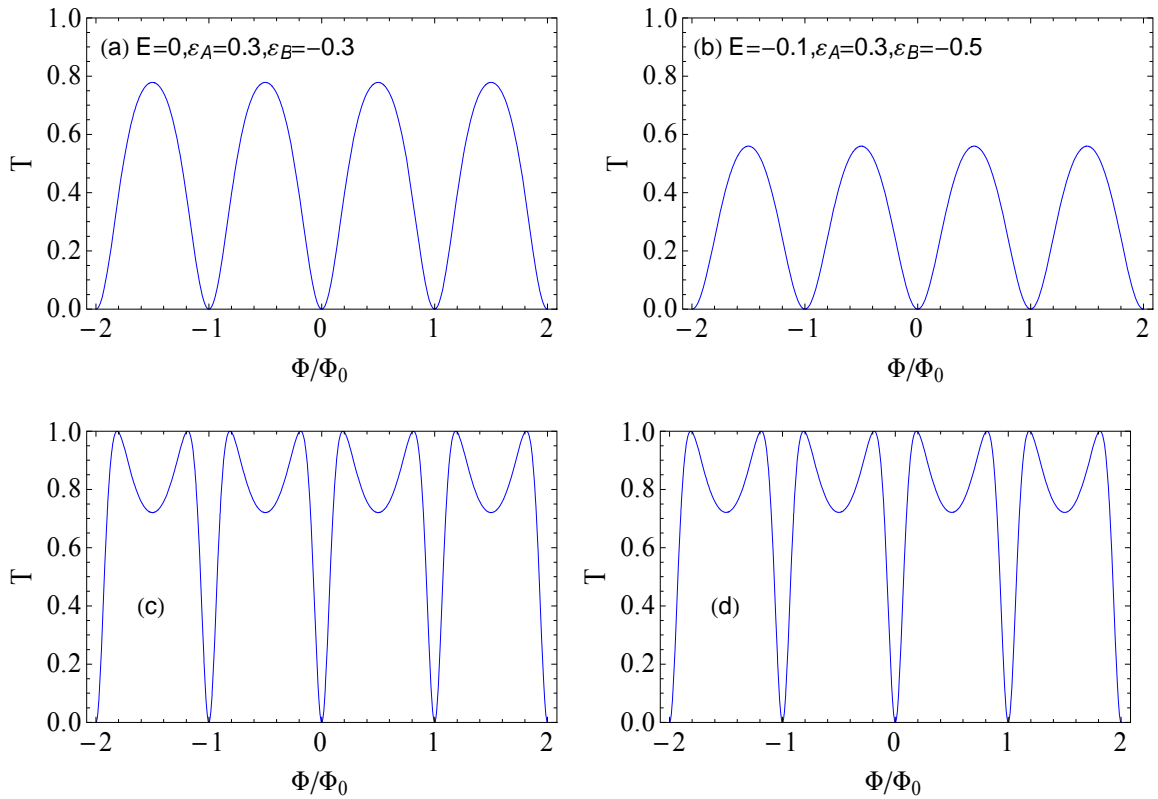


Figure 4.8 Suppressed transmissions occur at integer  $\Phi / \Phi_0$  when incident energy approaches to the average of two QDs energy values. In each case  $E = (\varepsilon_A + \varepsilon_B)/2$ , the shape of transmission of (c)  $E=0.1, \varepsilon_A = 0, \varepsilon_B = 0.2$  is identical to (d)  $E=0, \varepsilon_A = 0.1, \varepsilon_B = -0.1$ . These are all plotted at  $v_j=0$  and  $V_1=0.3$ .

Let us take a closer look at Fig. 4.8(c) and (d). They have identically the same transmission patterns despite different energy states. We find, however, that they have in common the difference of their two discrete dot energies.

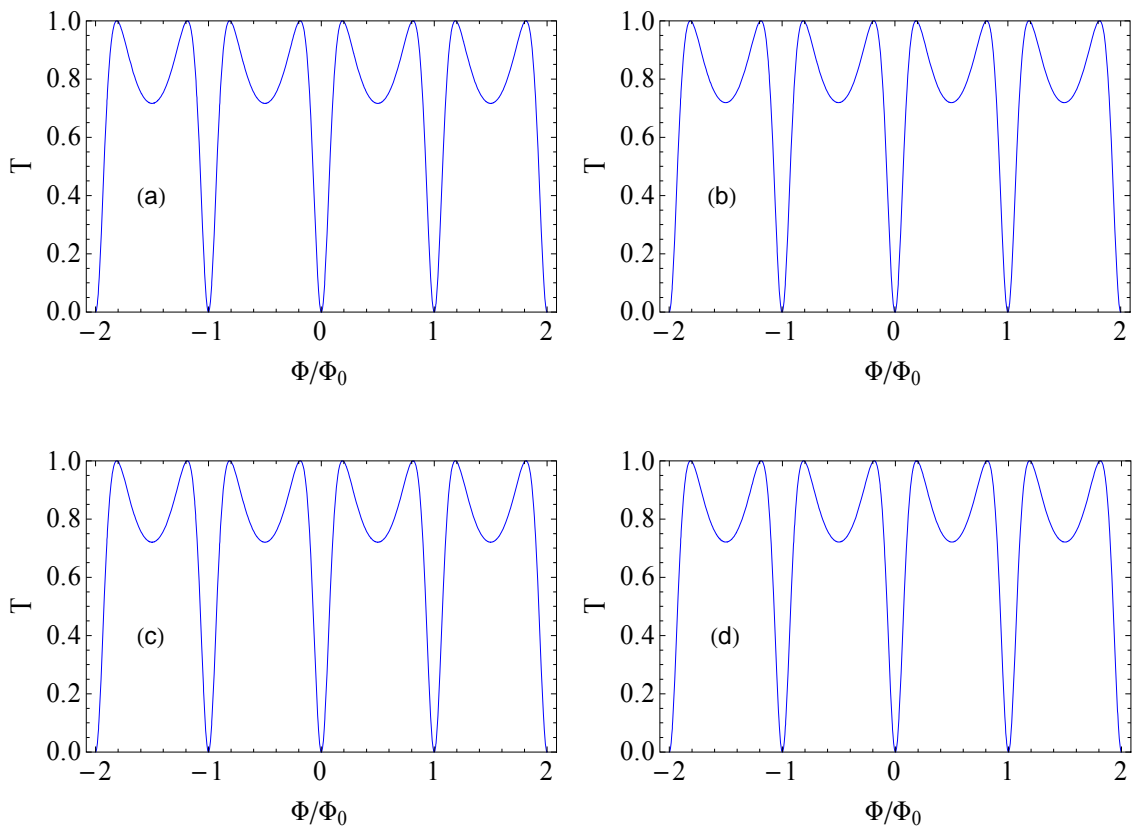


Figure 4.9 Identical AB oscillations of the transmission at  $E = \bar{\varepsilon}$  for some QD energy level difference. The QD parameters are changed from (a) to (d):  $(E, \varepsilon_A, \varepsilon_B) \rightarrow$  (a) (0.3, 0.2, 0.4), (b) (0.2, 0.1, 0.3), (c) (0.1, 0, 0.2), (d) (0, -0.1, 0.1).

Figure 4.9 shows that AB oscillations of transmission generate the same patterns when the difference of the two discrete levels in each dot is fixed with

$\Delta\varepsilon = \varepsilon_B - \varepsilon_A = 0.2$ , while the incident energy is set at the average of the two dot levels. When magnetic flux penetrates the ring, the suppressed oscillations of  $T(\varphi)$  occur when  $E = \bar{\varepsilon}$ . We can also observe identical AB oscillations with the tuned incident energy as long as the energy level difference of the two dots is same.

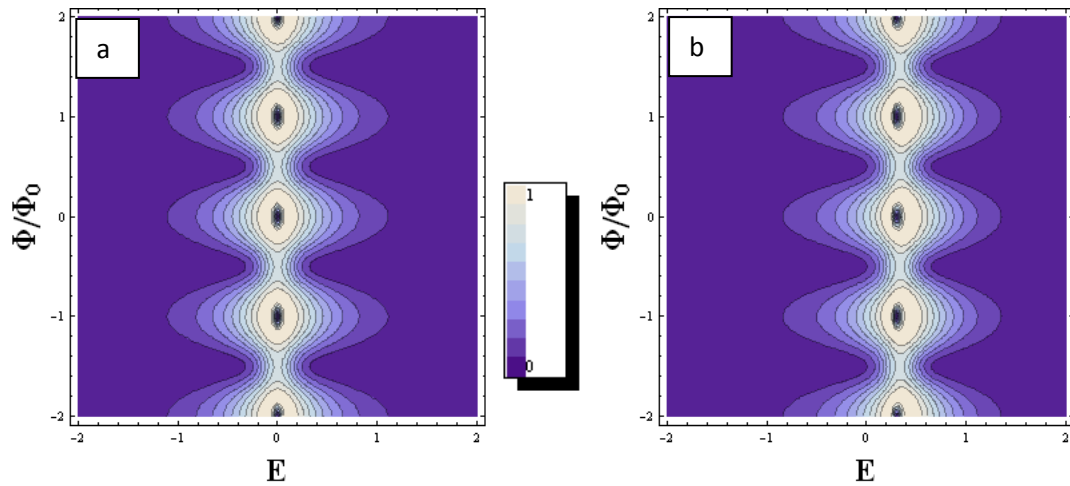


Figure 4.10 In contour plots of  $T(E, \varphi)$  the color scale indicates the magnitude of the transmission. The shape of two contours is identical except that the line of symmetry is shifted as two quasi-bound states are slightly changed from (a)  $\varepsilon_A = 0.1, \varepsilon_B = -0.1$  to (b)  $\varepsilon_A = 0.4, \varepsilon_B = 0.2$ .

Figure 4.10 shows contour plots of the electron transmission as functions of the magnetic flux in the  $y$  direction and the incident energy in the  $x$  direction. It reveals the AB oscillations of the transmission. Brighter regions account for the maximum transmission as the legend box between 4.10(a) and 4.10(b) illustrates the color of the transmission strength. The resonant shapes with different site energies have the same features even though the center of the resonant position shifts from  $E=0$  (Fig. 4.10(a)) to

the right (Fig. 4.10(b)). In both contour plots, the dark region, meaning  $T=0$ , is observed at  $E=\bar{\varepsilon}$  at every integer value of magnetic flux. So if we choose the incident energy to be at the average of two dots, the transmission goes to zero when we plot the  $T$  as a function of the magnetic flux for  $\Phi/\Phi_0 = \text{integer}$ .

If  $\varepsilon_A = \varepsilon_B = \varepsilon_0$ , sharpened AB oscillations in the transmission occur at  $E = \varepsilon_0$  [11]. Why does this suppressed transmission occur along the average value of two dots? It may be because in the absence of magnetic flux and inter-dot coupling, the position of the transmission zero is determined by  $E_0 = (\varepsilon_A + \varepsilon_B)/2$ . This means that an electron at the average energy value of the two dots does not participate in the resonant tunneling. Notice that if magnetic flux is applied,  $E_0$  only appears for  $\Phi/\Phi_0 = \text{integer}$ . Figure 4.11 topologically illustrates this for the case of a single potential well (QD) with two quasi-bound states.

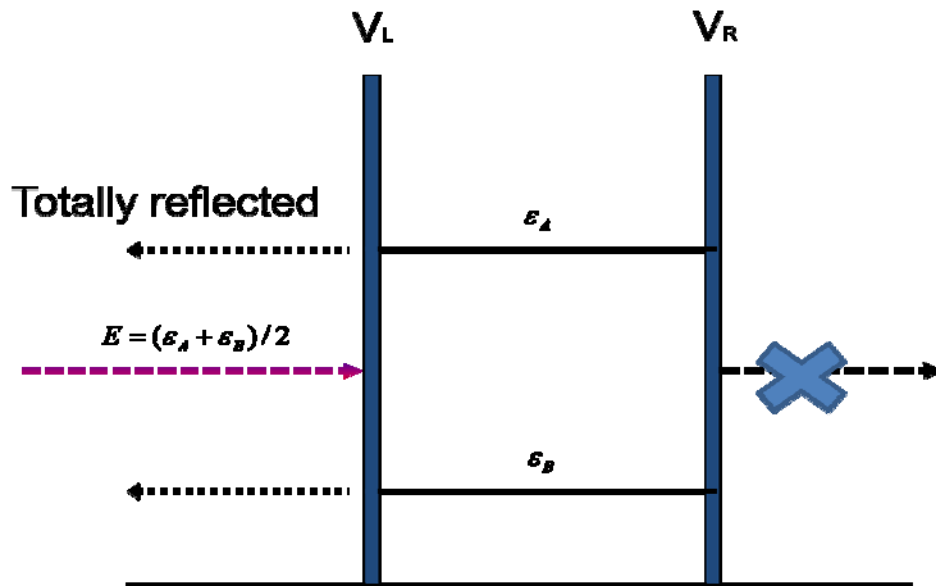


Figure 4.11 Schematic picture of total reflections when the magnetic flux  $\Phi/\Phi_0=0$  or integer and the incident energy meets the average energy value of the two dots.

#### 4.4 Inter-dot coupling effect

In our model, the inter-dot coupling is denoted by  $v_j$  (see Fig. 4.3). When the average of the dot energy levels is zero, the transmission zero is shifted by the amount of  $v_j$ . This may be expressed as

$$E_0 = \frac{\varepsilon_A + \varepsilon_B}{2} + v_j. \quad (4.7)$$

Figure 4.12 shows that the position of the transmission zero is determined by the inter-dot coupling, narrowing the antibonding resonant QD state.

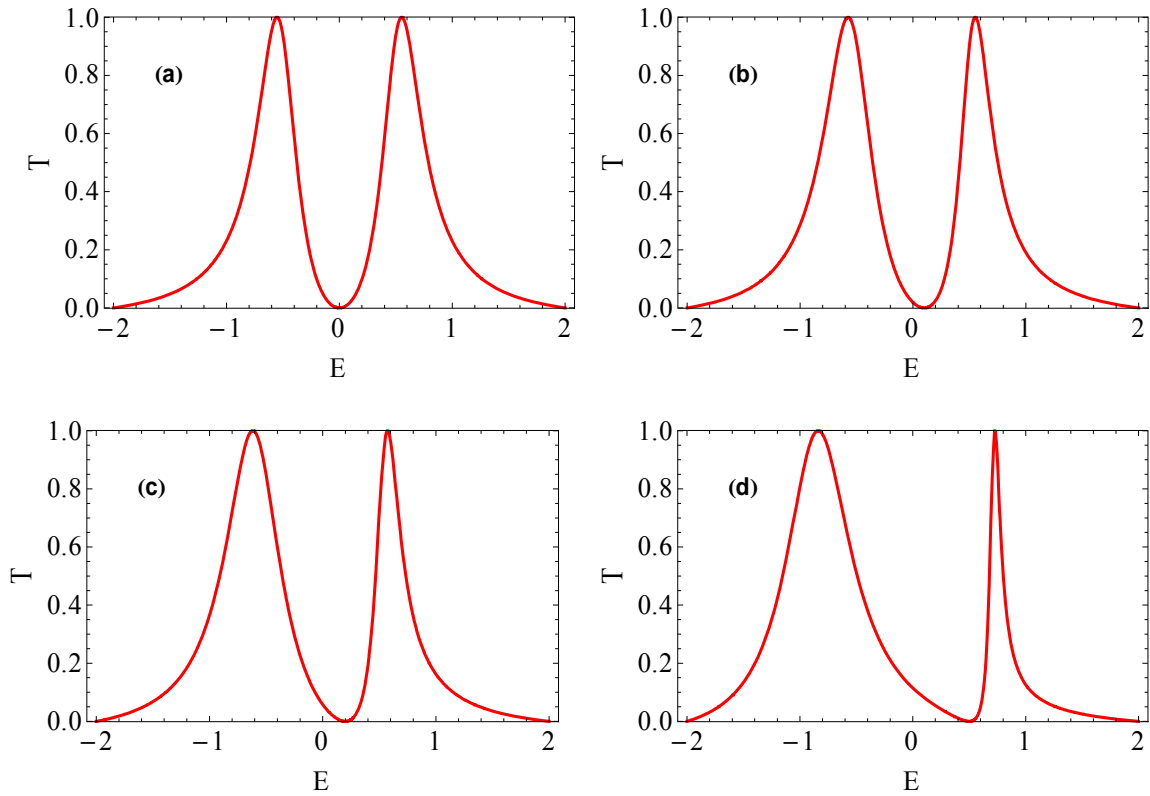


Figure 4.12 For the ring with symmetric arms in the absence of magnetic flux, the position of the resonance zero is given by  $E_0 = (\varepsilon_A + \varepsilon_B)/2 + v_j$ . Inter-dot coupling is varied from (a) to (d): (a) 0, (b) 0.1, (c) 0.2 and (d) 0.5. The other QD parameters are fixed at  $V_1 = 0.3$ ,  $\varepsilon_A = 0.5$ ,  $\varepsilon_B = -0.5$ , and  $\Phi = 0$ .

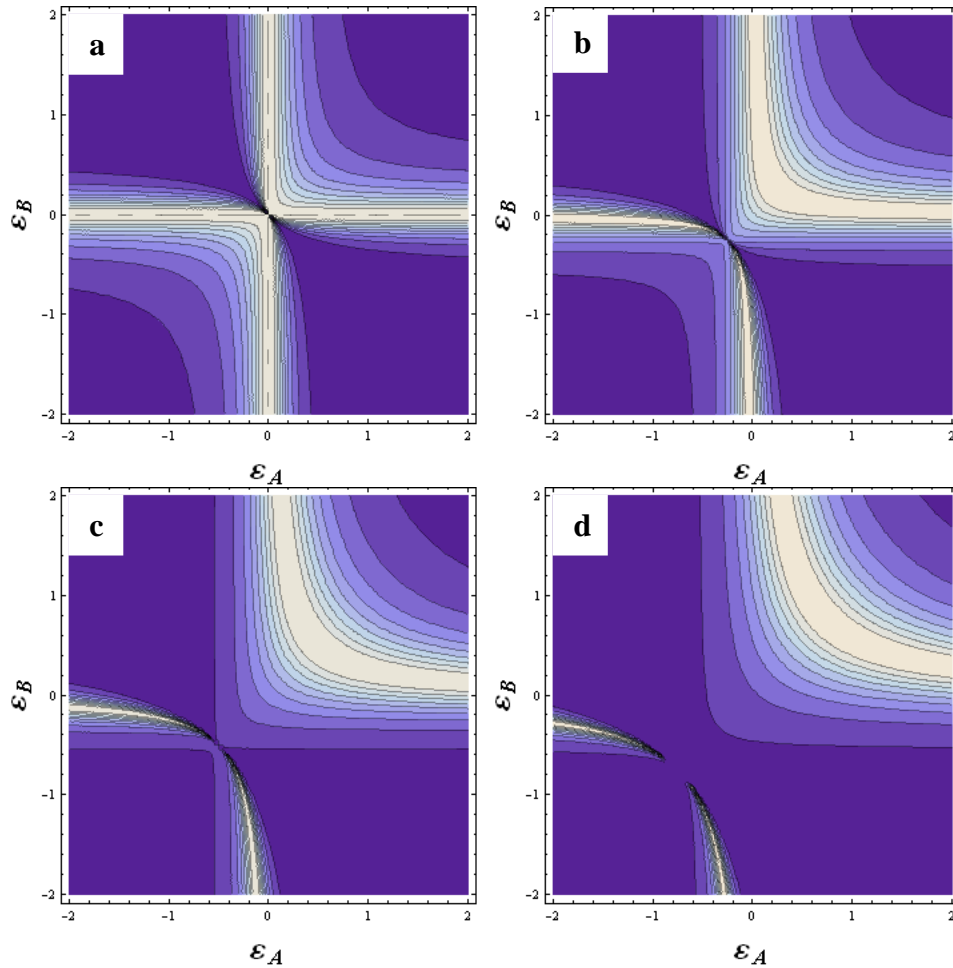


Figure 4.13 As  $v_j$  increases the lattice-like resonance loses intersection domains. From (a) to (d),  $v_j$  is increased:  $v_j =$  (a) 0, (b) 0.25, (c) 0.5, and (d) 0.75. Other parameters are fixed at  $E=0$ ,  $V_1=0.3$ , and  $V_0=1$ .

Figure 4.13 shows the contour plots of the transmission as functions of  $\epsilon_A$  and  $\epsilon_B$  as  $v_j$  is increased. At weak coupling<sup>1</sup>, the electron separately tunnels through the nearly

<sup>1</sup> Meaning when  $v_j$  is relatively smaller than lead-dot coupling. The ‘weak coupling’ includes  $v_j < 0.3$  since  $V_1$  is fixed at 0.3.

independent dots. With increasing  $v_j$ , the isolated quasi-bound state in each dot is gradually lost, and as shown in Fig. 4.13(c) and (d) the cross lines separate and the rectangular domain undergoes deformation. This is because at large  $v_j$  the electron pathway between the two dots is bigger, so the two dots merge into one. It's interesting to refer to Fig. 4.14(b) [27], experimentally showing the same inter-dot coupling effects in which the domain boundaries become straight lines from 1 to 4 (Fig. 4.14(b)). Notice that in our model, two coupled QDs make one rectangular domain at weak coupling, but in Fig. 4.14 multiple states in each dot induce the multiple cross sections.

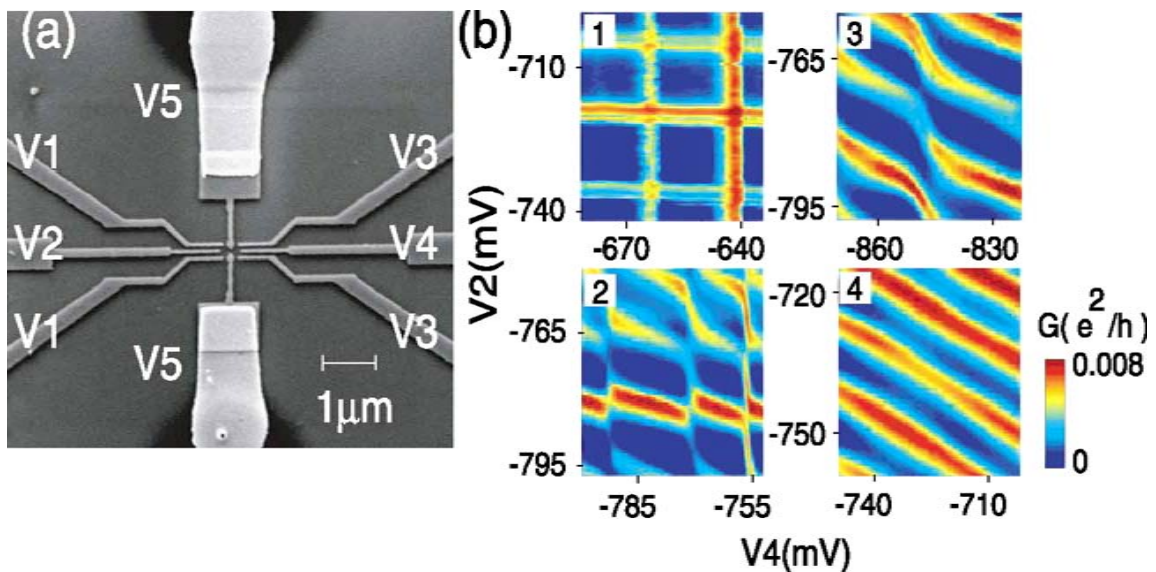


Figure 4.14 (a) Scanning electron micrograph of parallel double QDs. The lithographic size of each dot is 170nmx200nm. (b) Logarithm of double QD conductance as a function of  $V_2$  and  $V_4$  with different couplings. The inter-dot coupling is increased from (1) to (4).

We also found that the inter-dot coupling changes the periodicity of AB oscillations. The periodicity in Fig. 4.15(b) has been multiplied by 2 times as the inter-dot coupling is increase. The added phase difference induced by inter-dot coupling might produce changes in the period of the AB oscillations.

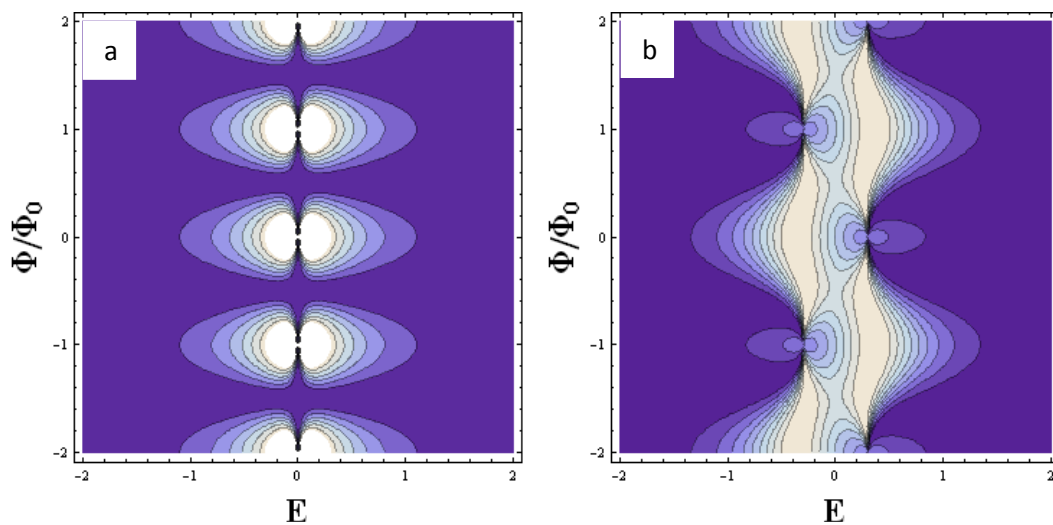


Figure 4.15 (a) AB oscillations are repeated every integer for  $v_j=0$ . (b) The periodicity of AB oscillations is changed to two flux quantum with a finite inter-dot coupling:  $v_j=0.3$ . The other QD parameters are fixed at  $E=0$ ,  $V_1=0.3$ , and  $V_0=1$  for identical QD ( $\epsilon_A=\epsilon_B=0$ ).

#### 4.5 Suppressed and maximized transmission

To begin with, let us focus on Fig. 4.16, a contour plot of the transmission versus  $\epsilon_A$  and  $\epsilon_B$ . Making a cut at  $\epsilon_B=0.1$  along the dotted red line in Fig. 4.16(a) gives the transmission curve in Fig. 4.16(b). As we saw in Fig. 4.11, the suppressed transmission,

( $T=0$ ) occurs at  $E=\bar{\varepsilon}$ . If we arbitrarily choose the value of the incident energy at  $E=0$ , then the yellow line in Fig. 4.16(a), representing  $\varepsilon_A = -\varepsilon_B$ , satisfies  $E=\bar{\varepsilon}$  in the absence of magnetic flux and inter-dot coupling. Therefore the yellow line indicates the suppressed transmission, i.e.,  $T(E=\bar{\varepsilon})=0$  along the reverse-diagonal direction. The calculation procedure to find the zero transmission is introduced in Appendix B. This suppressed transmission triggers the Fano resonance with its full transmission zero along the reversed diagonal line. If we cut at the small value of  $\varepsilon_B$  (dotted red line), the typical Fano resonance is observed as shown in Fig. 4.16(b). We observe the swing of Fano resonances in Fig. 4.17, showing that the Fano dip-peak pair is changed to a peak-dip pair with different site energy,  $\varepsilon_B$ .

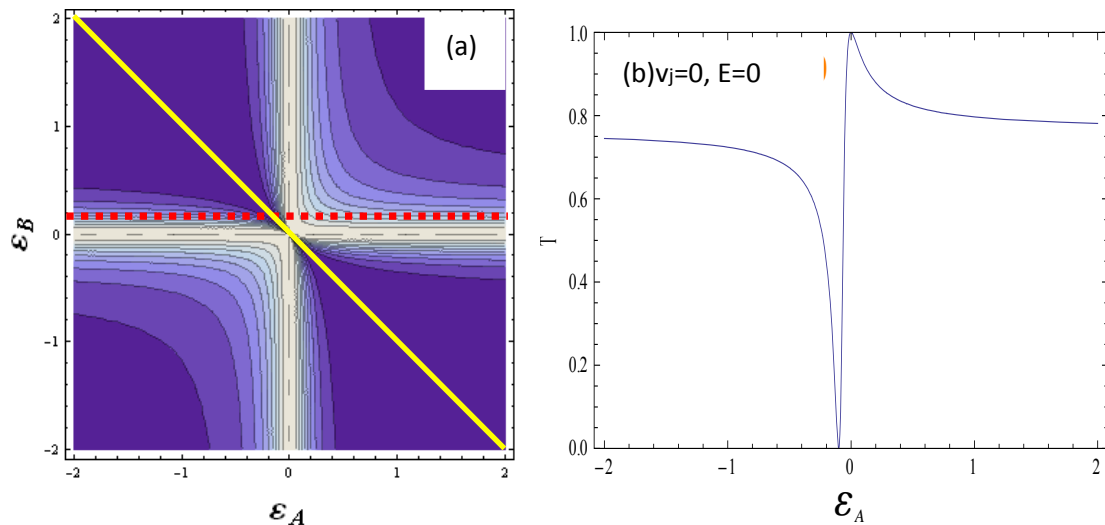


Figure 4.16 At fixed  $\varepsilon_B$ , the Fano resonance is observed because of the suppressed transmission along the yellow line of  $\bar{\varepsilon} = \varepsilon_A + \varepsilon_B = 0$ . Two plots above are generated for the case with symmetric arms,  $V_1=0.3$ . For (b),  $\varepsilon_B$  is fixed at 0.1 and  $V_0=1$ . QD parameters are applied to both (a) and (b):  $v_j=0$ ,  $E=0$ , and  $\Phi=0$ .

The center in Fig. 4.16(a) is a totally transmitted region where  $\varepsilon_A = \varepsilon_B = E$ , giving rise to the confirmation that the transmission peak depends on the quasi-bound states. The work to show  $T=1$  at the singular point  $(\varepsilon_A, \varepsilon_B, E) = (0, 0, 0)$  is shown in Appendix C, which proves that the central area in Fig. 4.16(a) indicates the maximized transmission, although the zero transmission is observed along the reversed diagonal line. At the singular point  $\varepsilon_A = 0$  and  $\varepsilon_B = 0$ , the suppressed transmission along the line  $\varepsilon_B = -\varepsilon_A$  (for  $E = (\varepsilon_A + \varepsilon_B)/2 = 0$ ) conflicts with the earlier result that the transmission peak,  $T=1$ , occurs at  $E = \varepsilon_A = \varepsilon_B = 0$ . Note that in this case Eq. (4.7) is no longer valid.

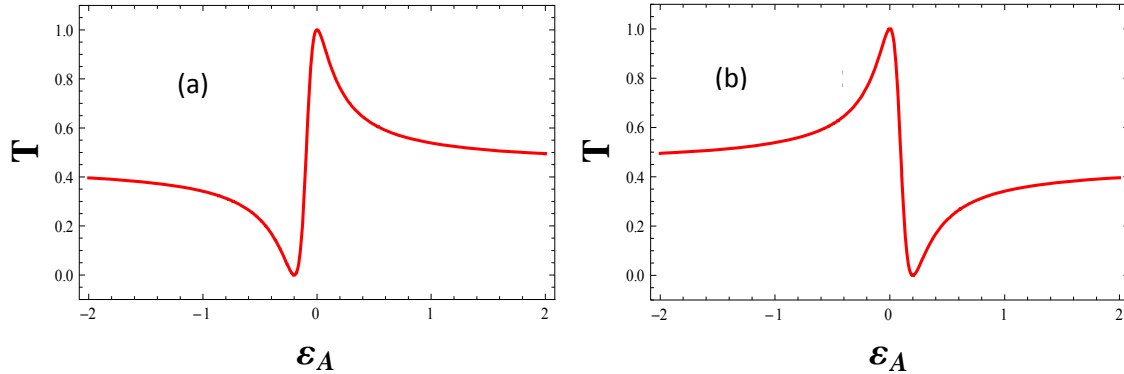


Figure 4.17 (a) The Fano dip-peak is changed to a peak-dip pair (b) in the Fano resonance as one of the dot energies is changed: (a)  $\varepsilon_B = 0.2$  and (b)  $\varepsilon_B = -0.2$ .

## Chapter 5: Transmission through multiple states in a coupled quantum dot

### 5.1 Introduction

Resonance features in the vicinity of each quasi-bound state have been studied for the coupled double QD in which each has a single state. However, it is interesting to consider multiply connected states which are dealt with Ref. [27]. Recently the two-level model for a double QD coupled to two leads of spinless electron was studied in Ref. [28], in which V. Kashcheyevs *et al.* feature arbitrary tunneling matrix elements among two levels and the leads and between the levels themselves. In this chapter, we analyze interference effects with an embedded multi-state-QD in symmetric arms of an AB ring, where each state is linked to the other two states of the opposite QD with inter-dot couplings  $v_{n,m}$ .

Employing the exactly solvable formalism of the tight-binding model (Eq. (4.2)), electron transport in an AB ring can be observed and manipulated by controlling QD parameters, including inter-dot couplings,  $v_{db}, v_{da}, v_{cb}$  and  $v_{ca}$ , and magnetic flux. Note that, in this model, two states in each dot are coupled to the other two states and each coupling can be tuned independently. For example,  $v_{db}$  means the coupling between states  $d$  and  $b$  and we can tune only  $v_{db}$  without affecting other couplings.

In this study, we tune the inter-dot couplings to show that charging inter-dot couplings shifts the position of the Breit-Wigner and Fano resonances. Next we move on to find the position of the transmission zero,  $E_0$ , as a function of incoming energy, in the absence of magnetic flux. Figure 5.1 is a schematic of bi-level QD embedded in an AB ring. There are two quasi-bound states in each dot. Let us call the lower state an ‘even state’ and the upper state an ‘odd state’. Two identical dots are located at the middle of the arms, where each state is coupled to other states in another identical dot with tunable inter-dot couplings  $v_{n,m}$ . When lead-dot couplings are given as  $V_{dl} = V_{cl} = V_{bl} = V_{al} = V_{ar} = V_{br} = V_{cr} = V_{dr} = V_1$ , we have a symmetrical parallel ring (see Fig. 5.1).

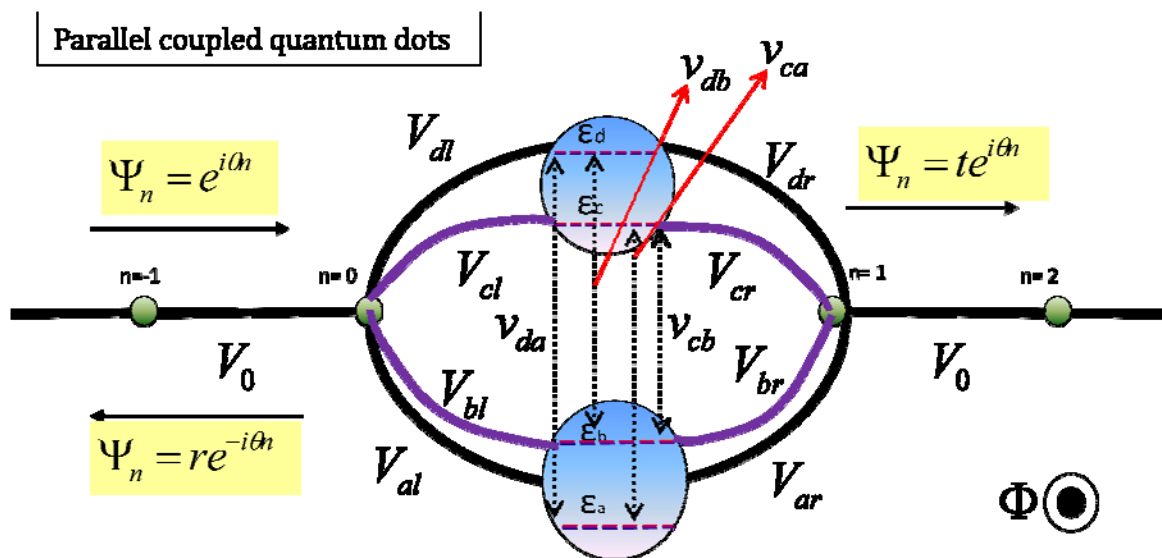


Figure 5.1 Schematic of the two energy states in double quantum dots. Each state is coupled to other states with different coupling strengths. In addition to the magnetic flux  $\Phi$  threading the AB ring, the relevant coupling parameters between sites are defined.

## 5.2 Formalism

When discretized energy states are coupled by different coupling strengths in Fig. 5.1, the Schrodinger equation in the tight-binding approximation can be written as  $-\sum V_{n,m}\psi_m + \varepsilon_n\psi_n = E\psi_n$ . As we described in chapter 4, system parameters are introduced for the nearest-neighbor couplings to site  $n$ , where  $\varepsilon_n$  is the site energy and  $E$  is the electron energy. In our calculation, the site energies  $\varepsilon_n$  are set to zero for all sites except for the QDs. The parameters  $V_{n,m}$  are used as overlap integrals. In the homogeneous leads, the coupling parameters are all set to  $V_0 = 1.0$  as used in chapter 4, which we use throughout discussion as a unit of energy [5]. In the presence of magnetic flux  $\Phi$ , we choose a gauge in which the coupling parameter for each segment of the arm is modified as  $V_{nm} \rightarrow V_{nm}e^{\pm i\varphi}$ . The plus sign is for counterclockwise transport and the minus sign is for clockwise transport around the ring. The phase  $\varphi$  is related to the magnetic flux  $\Phi$  by  $4\varphi = 2\pi\Phi/\Phi_0$ , where  $\Phi_0 = h/e$  is the flux quantum. After some work (see Appendix D), we derive the transmission amplitude with some conditions<sup>1</sup>:

$$t = \frac{-2ie^{2i\theta}V_1^2\{4E^3 - \varepsilon_a\varepsilon_b\varepsilon_c - \varepsilon_a\varepsilon_b\varepsilon_d - \varepsilon_b\varepsilon_c\varepsilon_d - 3E^2(\varepsilon_a + \varepsilon_b + \varepsilon_c + \varepsilon_d) + 2E[\varepsilon_c\varepsilon_d + \varepsilon_b(\varepsilon_c + \varepsilon_d) + \varepsilon_a(\varepsilon_b + \varepsilon_c + \varepsilon_d)]\}\sin\theta}{E^4V_0 + V_0\varepsilon_a\varepsilon_b\varepsilon_c\varepsilon_d + E^3[8e^{i\theta}V_1^2 - V_0(\varepsilon_a + \varepsilon_b + \varepsilon_c + \varepsilon_d)] - 2e^{i\theta}V_1^2\{\varepsilon_b\varepsilon_c\varepsilon_d + \varepsilon_d[\varepsilon_c\varepsilon_d + \varepsilon_b(\varepsilon_c + \varepsilon_d)]\} + E^2(\dots)} E(\dots). \quad (5.1)$$

<sup>1</sup> Eq. (5.1) is derived under the condition that there is no direct inter-dot coupling on magnetic flux in a symmetric ring ( $V_{la} = V_{lb} = V_{lc} = V_{ld} = V_{rd} = V_{rc} = V_{rb} = V_{ra} = V_1$ ).

Figure 5.2 shows the resonant features for four different quasi-bound states. As we can see in Eq. (5.1), the resulting transmission amplitude given as a function of electron energy,  $E$ , is expressed as

$$t(E) = \frac{N(E)}{D(E)}. \quad (5.2)$$

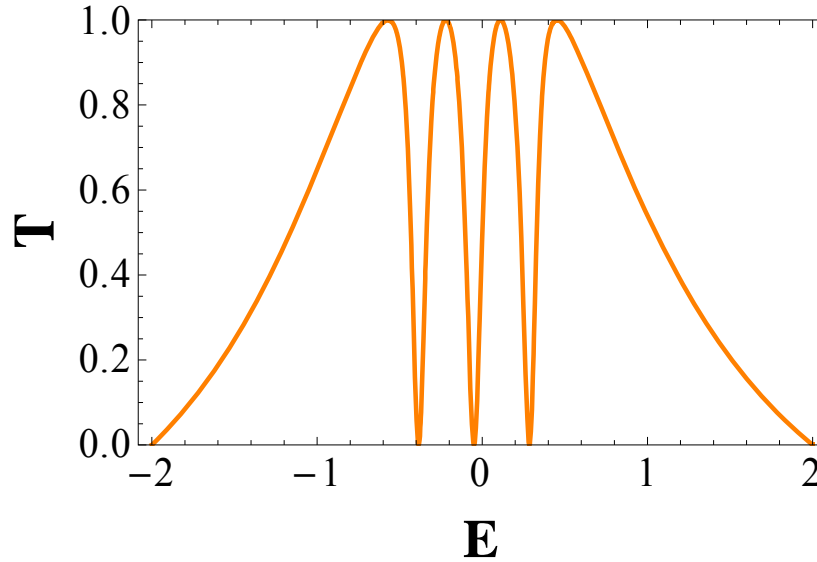


Figure 5.2 Each resonant state represents four quasi-bound states with the conditions of  $V_1 = 0.3$ ,  $\Phi = 0$ , no inter-dot couplings ( $v_{da} = v_{db} = v_{cb} = v_{ca} = 0$ ), and ( $\varepsilon_a = 0.5$ ,  $\varepsilon_b = -0.2$ ,  $\varepsilon_c = 0.1$  and  $\varepsilon_d = 0.4$ ).

The transmission amplitude will be zero when the numerator goes to zero<sup>1</sup>. The numerator is a cubic equation for  $E$  so that there are three solutions to satisfy the equation<sup>2</sup>, which is the reason why there are three zeros in Fig. 5.2. We find these  $E_0$  by setting  $N(E)=0$  which gives  $-0.385$ ,  $-0.05$  and  $0.285$ . These three values are well matched with  $E_0$  in Fig. 5.2.

<sup>1</sup> $D(E)$  doesn't go to infinity.

<sup>2</sup>The lead-dot coupling  $V_1$  is not zero, and  $\sin\theta \neq 0$ .

### 5.3 Identical QDs.

We assume that there are two identical quantum dots, that is, ( $\varepsilon_d = \varepsilon_b$  and  $\varepsilon_c = \varepsilon_a$ ). All couplings are tuned together as if they are one ( $v_{db} = v_{da} = v_{cb} = v_{ca} = v_j$ ). In this case, the transmission amplitude can be more simply expressed as<sup>1</sup>

$$t = \frac{-4ie^{2i\theta}V_1^2(2E - \varepsilon_a - \varepsilon_b)\sin\theta}{E^2 + E(8e^{i\theta}V_1^2 - \varepsilon_a - \varepsilon_b) + \varepsilon_a\varepsilon_b - 4e^{i\theta}V_1^2(\varepsilon_a + \varepsilon_b) + v_j(2E - \varepsilon_a - \varepsilon_b)}. \quad (5.3)$$

Notice that Fig. 5.3 shows the transmission probability versus the incident energy when the QDs both have two of the same quasi-bound states:  $\varepsilon_d = \varepsilon_b = 0.2$  and  $\varepsilon_c = \varepsilon_a = -0.2$ . Figure 5.3 features the case when all of the inter-dot couplings are equally applied. The position of the peaks is shifted to lower energy when the homogeneous inter-dot couplings are turned on with the same values (see Fig. 5.3). However,  $E_0$  remains the same at zero, while the peak on the right side starts to show a Fano-type resonance. So, is  $E_0$  independent of the inter-dot couplings even though, based on our study of a single state with inter-dot coupling, the transmission zero depends on the inter-dot coupling? It is because the numerator doesn't include the inter-dot coupling term in Eq. (5.3). Only the denominator includes the inter-dot coupling term. Therefore increasing  $v_j$  doesn't change the position of  $E_0$  but it does affect the peaks. This is because the position of

---

<sup>1</sup> For simplicity,  $V_0 = 1$  as a unit energy, is plugged into Eq. (5.1).

resonance peaks is determined by the denominator of the transmission amplitude ( $D(E)=0$ ). Figure 5.4 confirms that, for equally tuned coupled identical QDs,  $E_0$  is only determined by two quasi-bound states  $\varepsilon_a$  and  $\varepsilon_b$  in the absence of magnetic flux, assuming that lead-dot couplings always exist.

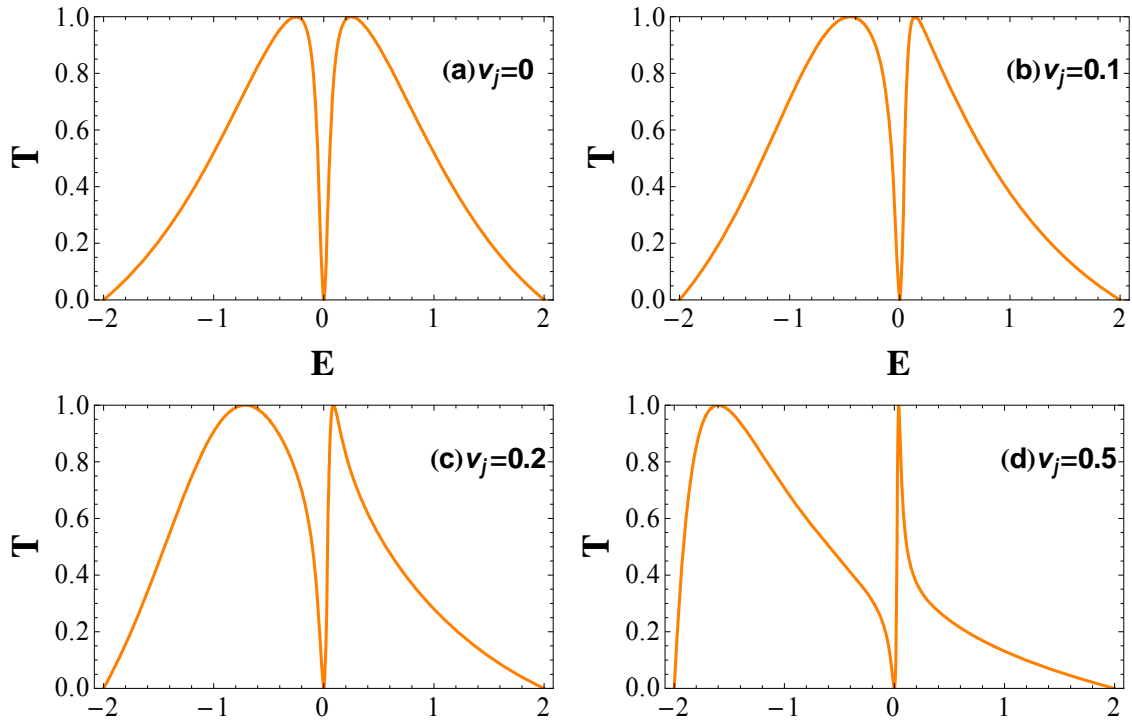


Figure 5.3 Resonance peaks through two identical quantum dots ( $\varepsilon_d = \varepsilon_b = 0.2$ ,  $\varepsilon_c = \varepsilon_a = -0.2$ ) in a symmetric AB ring in the absence of magnetic field are shifted to lower energy as all inter-dot couplings ( $v_{db} = v_{da} = v_{cb} = v_{ca} = v_j$ ) are simultaneously increased while the transmission zero,  $E_0$ , remains the same, despite the interaction between quasi-bound states ( $V_0 = 1, V_1 = 0.3, \Phi = 0$ ).

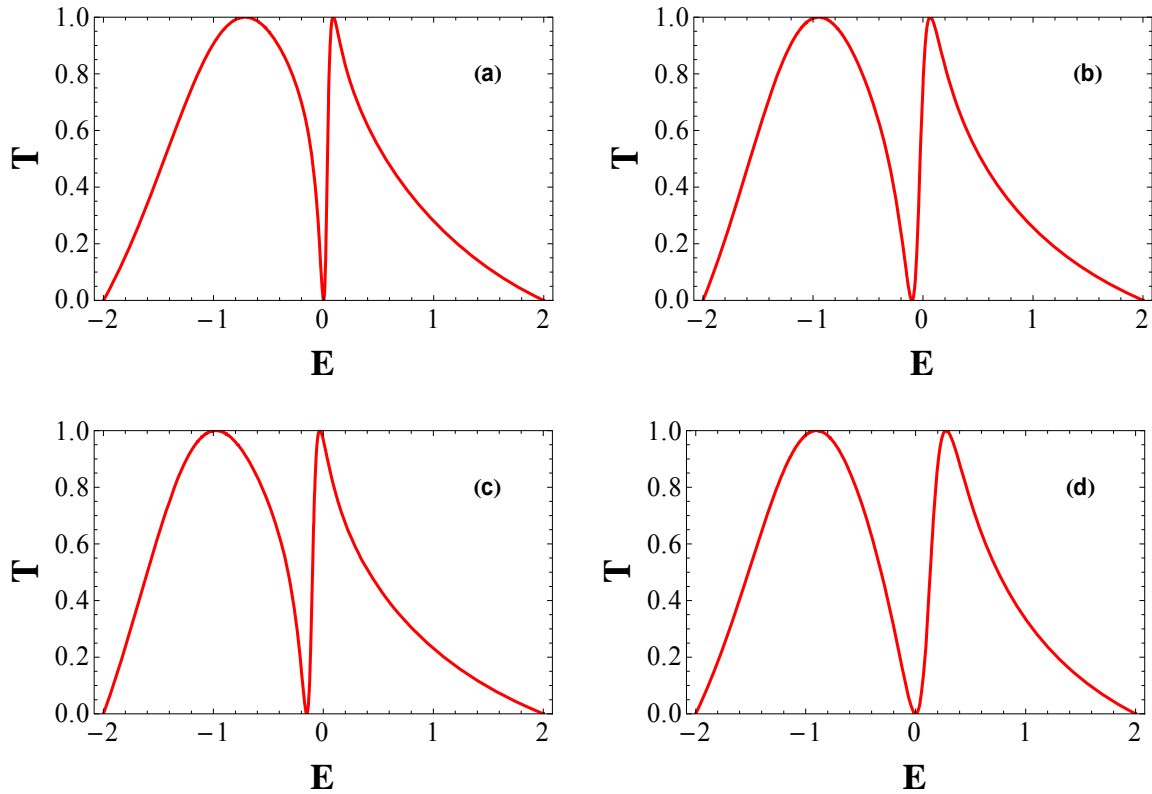


Figure 5.4 For the case with  $V_1=0.3$ ,  $\Phi_0=0$ , and inter-dot couplings ( $v_{da} = v_{db} = v_{cb} = v_{ca} = v_j = 0.2$ ), as two bound state energies are varied:  $(\varepsilon_a, \varepsilon_b) \rightarrow$  (a) $=(-0.2, 0.2)$ , (b) $=(-0.4, 0.2)$ , (c) $=(-0.4, 0.1)$ , (d) $=(-0.4, 0.4)$ ,  $E_0$  depends only on the two bound state energies,  $\varepsilon_a$  and  $\varepsilon_b$ .

#### 5.4 Inter-dot coupling between the higher-level states, $v_{db}$

Assume that there are two identical QDs which have two quasi-bound states embedded in an AB ring. In order to find the effects of each single inter-dot coupling on the transmission, we fix the other inter-dot couplings at zero and vary only the one of inter-dot coupling. First, we examine the interaction between states  $d$  and  $b$  - upper energy

states, (called *odd states*) when the lead-dot couplings maintain symmetric arms. Then,

Eq. (5.1) can be simplified to

$$t = \frac{4ie^{2i\theta}V_1^2(2E + v_{db} - \varepsilon_a - \varepsilon_b)\text{Sin}\theta}{E^2 + 4e^{i\theta}V_1^2(v_{db} - \varepsilon_a - \varepsilon_b) + E(8e^{i\theta}V_1^2 + v_{db} - \varepsilon_a - \varepsilon_b) + (\varepsilon_b - v_{db})\varepsilon_a}. \quad (5.4)$$

In order to find the inter-dot coupling,  $v_{db}$ , between *odd states*, we plot the transmission probability as a function of the incident energy,  $E$ , when only  $v_{db}$  is tuned. Then, we observe the trend with increasing  $v_{db}$ .

Initially, as seen in Fig.5.5, there are two resonance peaks,  $E_p$  at  $E = -0.2$  for  $\varepsilon_a$  and  $\varepsilon_c$ , and at  $E = 0.2$  for  $\varepsilon_b$  and  $\varepsilon_d$ . By increasing  $v_{db}$ ,  $E_p$  (on the right) is slightly shifted to lower energy while the  $E_p$  (on the left) remains the same. It seems that the inter-dot coupling only lowers the quasi-bound state energy of the states connected by the coupling because the resonant transmission phenomena are related to the quasi-bound states in QDs; that is, increasing inter-dot couplings effectively lowers the QD's energy states independently. Finally, at  $v_{db} = 0.4$ , the two peaks are overlapped as one. How does this resonant state transit to the other state? In our research, we can predict the change of the quasi-bound state. For  $v_{db} > 0.4$ , the upper resonant peak crosses over and becomes the lower resonant peak.

It is also interesting to trace  $E_0$  in order to explain it numerically. From Eq. (5.4), we can find  $E_0$  in the absence of magnetic field when other inter-dot couplings are zero except  $v_{db}$ . It becomes

$$E_0 = \frac{1}{2}(-v_{db} + \varepsilon_a + \varepsilon_b) . \quad (5.5)$$

Notice that  $E_0$  is determined by the inter-dot coupling between higher states, called odd states, when quasi-bound state energies are fixed, which explains the trend shown in Fig. 5.5.

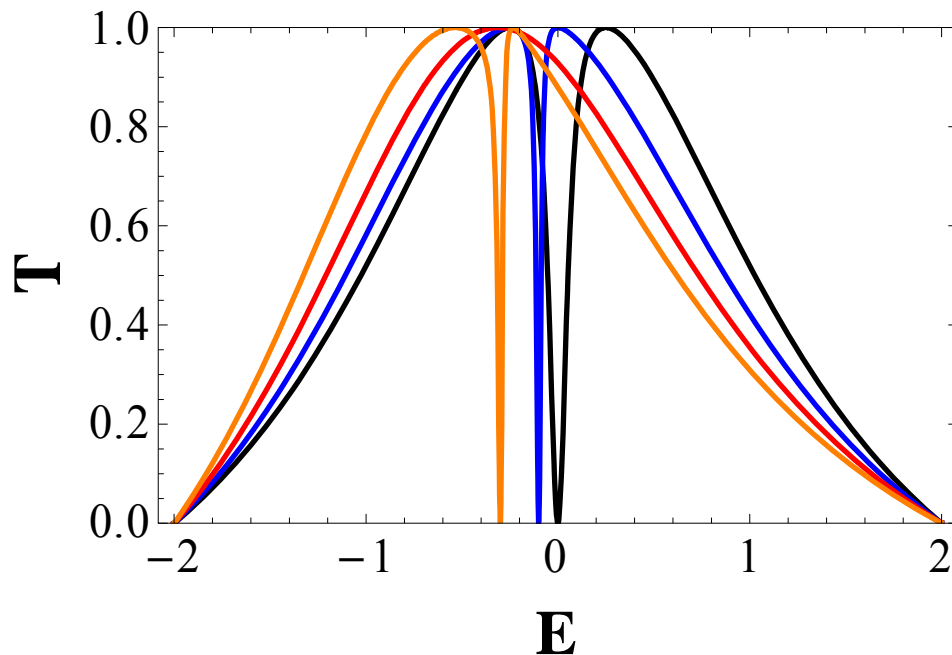


Figure 5.5 Transmission plots with the increase of  $v_{db}$  from black, blue, red, and orange (right to left for  $E > 0$ ) with (0, 0.2, 0.4, 0.6). Other couplings are zero ( $v_{da} = v_{cb} = v_{ca} = 0$ ).

### 5.5 Inter-dot coupling $v_{ca}$

Let's study the case when the inter-dot coupling is applied only between the low-energy states (even states). According to our study in the previous section, the separation of the full transmission peaks will be larger because the resonant state on the left continuously moves to lower energy. If we take a look at Fig. 5.6, as we expect, only the low-energy peak is shifted to lower energy. In contrast, the resonance peak on the right side keeps its position (see Fig. 5.6). We can conclude that increasing inter-dot coupling  $v_{ca}$  lowers the energy of the even quasi-bound states.

From Eq. (5.1), the transmission amplitude for this case (only with  $v_{ca}$ ) can be simplified to

$$t = \frac{4ie^{2i\theta}V_1^2(2E + v_{ca} - \varepsilon_a - \varepsilon_b)\text{Sin}\theta}{E^2 + 4e^{i\theta}V_1^2v_{ca} + E(8e^{i\theta}V_1^2 + v_{ca}) + (\varepsilon_a - v_{ca})\varepsilon_a} . \quad (5.6)$$

Setting the numerator equal to zero, when only inter-dot coupling,  $v_{ca}$ , is activated,  $E_0$  is

$$E_0 = \frac{1}{2}(-v_{ca} + \varepsilon_a + \varepsilon_b) . \quad (5.7)$$

We could say that increasing inter-dot coupling between identical states lowers their energy. In contrast to the odd-odd coupling ( $v_{db}$ ), increasing  $v_{ca}$  never results in the

annihilation of the resonant zero as happens with increasing  $v_{db}$  since there is no possibility of overlapping  $E_0$  with the higher energy resonant peak.

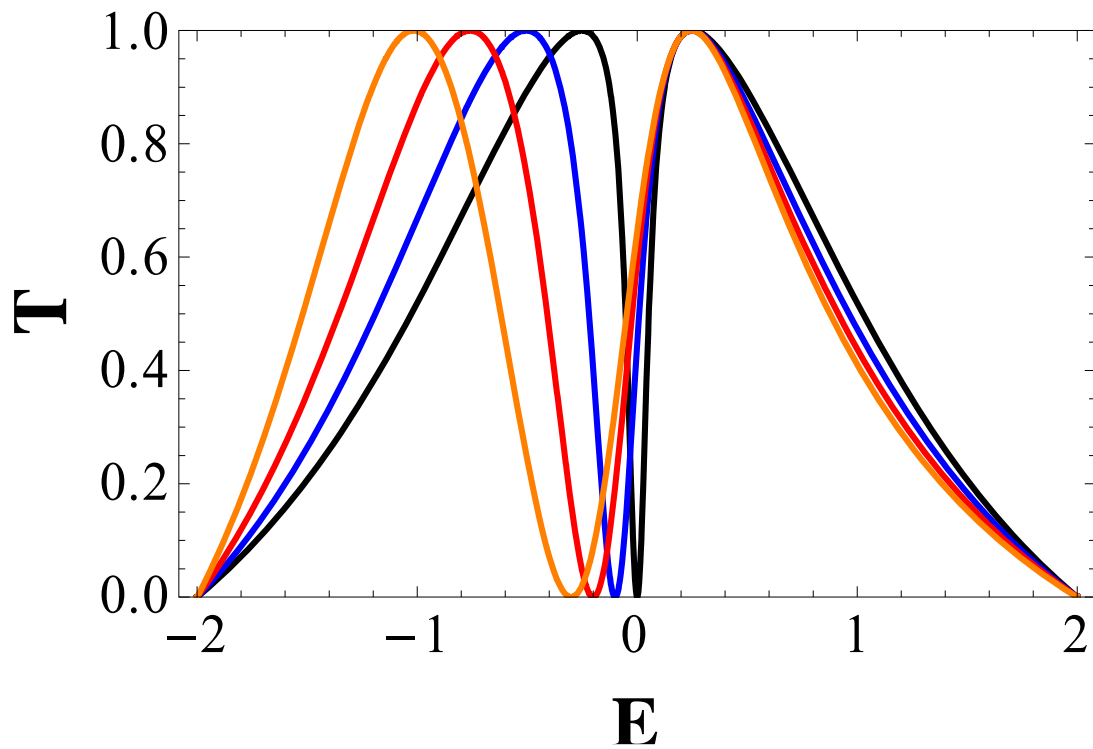


Figure 5.6 Transmission probability as a function of the incident energy for various  $v_{ca}$  : black, blue, red and orange (0, 0.2, 0.4, and 0.6) for  $v_{da} = v_{db} = v_{cb} = 0$ .

### 5.5 Even-odd, odd-even coupling

We observed the shape of the transmission with increasing the odd-odd state coupling, corresponding to  $v_{db}$ , and even-even inter-dot couplings,  $v_{ca}$ . For these cases, the mutual

interaction simply shifts the quasi-bound states. What if the interaction between even-odd or odd-even states is applied? Let us find the transmission amplitude  $t$  first.

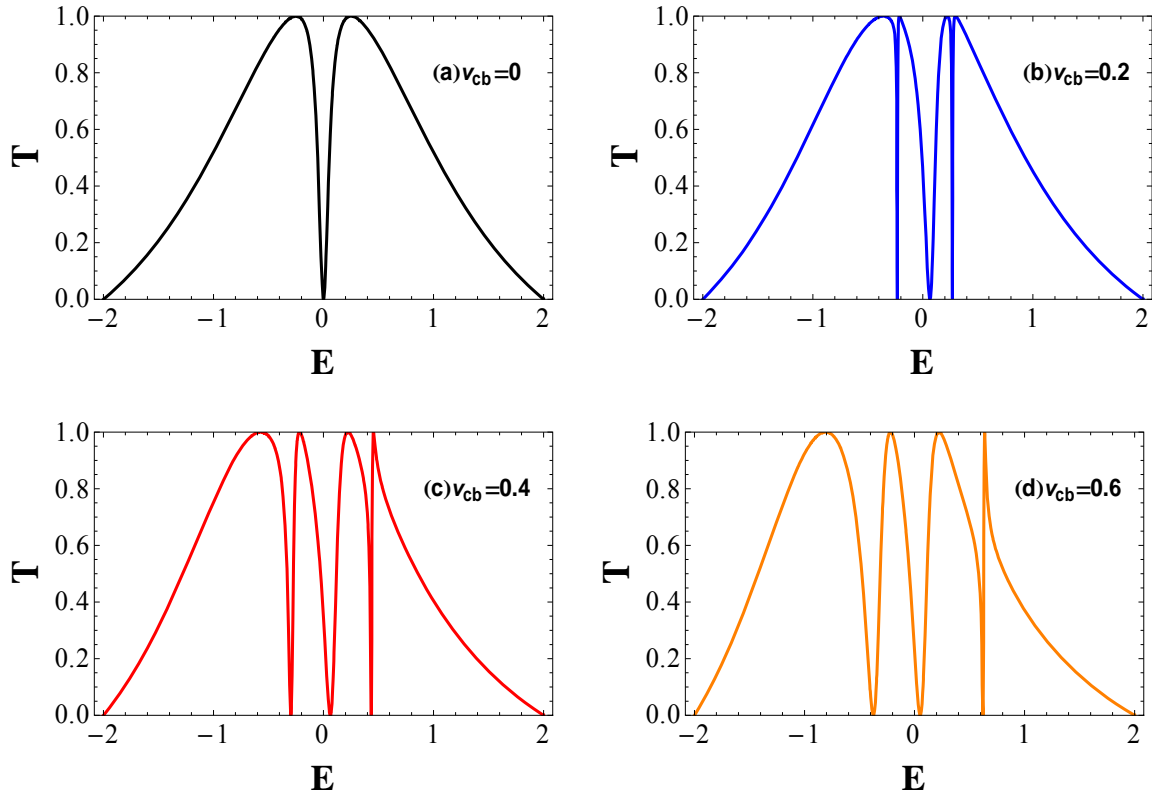


Figure 5.7 Even-odd interaction creating the other peaks indicates that additional bound states are formed, while the two peaks at 0.2,-0.2 remain the same. Other inter-dot couplings besides  $v_{cb}$  are fixed at zero in the absence of magnetic flux.

For  $v_{cb} \neq 0$  and  $v_{db} = v_{da} = v_{ca} = 0$ , Eq. (5.1) can be simplified to

$$t = \frac{2ie^{2i\theta}V_1^2(4E^3 - 2v_{cb}\varepsilon_a\varepsilon_b + v_{cb}^2(\varepsilon_a + \varepsilon_b) - 2\varepsilon_a\varepsilon_b(\varepsilon_a + \varepsilon_b) - 2E^2(v_{cb} + 3(\varepsilon_a + \varepsilon_b))\dots\dots}{E^4 + \varepsilon_a\varepsilon_b(\varepsilon_a\varepsilon_b - v_{cb}^2) + E^3(8e^{i\theta}V_1^2 - 2(\varepsilon_a + \varepsilon_b)) + 2e^{i\theta}V_1^2(-2v_{cb}\varepsilon_a\varepsilon_b + v_{cb}^2(\varepsilon_a + \varepsilon_b))\dots\dots} \quad (5.8)$$

Note that this is equivalent to the expression for odd-even inter-dot coupling,  $v_{da} \neq 0$  and  $v_{db} = v_{cb} = v_{ca} = 0$ . Looking at the numerator of Eq. (5.8), we find that it is a cubic equation and varied by  $v_{cb}$  so that there are three  $E_0$  values as shown in Fig. 5.7. Mutual interaction gives rise to the discrete energy levels between original levels. There are still only two bound states in the ring even after coupling is applied only between  $\varepsilon_c$  and  $\varepsilon_a$ , which share the same state. However, when  $v_{da}$  or  $v_{cb}$  is turned on without other couplings, additional states emerge so that two more peaks appear. So the total number of resonance peaks become four. This resonant phenomena can be explained with single state QD. Assuming that there is one quasi-bound state in each dot but with different states (Fig. 4.3), then tuning the inter-dot coupling makes an additional peak. So, we would say that whenever the inter-dot couplings between different states are increased, additional states arise.

## Chapter 6: Conclusion

In this thesis, we have explored a variety of properties of electron tunneling through coupled quantum dots in a ring structure by using the tight-binding Schrodinger equation. We have traced the electron transmission with varying system parameters which correspond to experimental investigations on these systems which often focus on current flowing between gates for different gate voltages [25], corresponding to varying the energy levels and coupling parameter.

Our investigation started with a 2DEG at the interface of a GaAs/AlGaAs. As the study progressed, we confirmed some results which correspond to the results of other researchers, showing that, (1) resonance tunneling is dependent on the quasi-bound state, (2) the Lorentzian half-width of the transmission peak,  $\Delta E$ , is related to the combined lifetime  $\tau$  for tunneling through either of the two enclosing lead-dot couplings<sup>1</sup>, and (3) AB oscillations have the periodicity of the flux quantum ( $h/e$ ), for the uncoupled QDs. During the study of AB oscillations for a single state in a dot, we found that (4) the transmission zero occurs when the value of incident energy is equal to the average of two states ( $E = (\varepsilon_a + \varepsilon_b)/2$ ). We also found that (5) the *periodicity* of the AB oscillations is

---

<sup>1</sup> Therefore, as in Eq. (3.26),  $U \propto 1/V_1$ , implies that the smaller value of dot-lead coupling, the longer lifetime of a quasi-bound state because  $\Delta E$  is narrower with decreasing  $V_1$ .

doubled for the case of non-zero inter-dot coupling. It is interesting to compare the effect of inter-dot coupling on the transmission zero in single quasi-bound state (Fig.4.3) with the inter-dot coupling effect<sup>1</sup> that occurs in two-state identical dots (Fig. 5.1). In the absence of magnetic flux the transmission zero is obtained for single state QDs, (6)

$E_0 = (\varepsilon_A + \varepsilon_B)/2 + v_j$ , while  $E_0$  for two-state identical QDs is defined as (7)

$$E_0 = \frac{1}{2}(-v_j + \varepsilon_a + \varepsilon_b).$$

In addition, considering the interaction between dissimilar states in the absence of magnetic flux, we found that (8) extra states arise as  $v_{da}$  or  $v_{cb}$  is tuned, as evidenced by the appearance of Fano resonances.

The parallel-coupled double QD in an AB-ring exhibits a rich depth of variability. Even though we have been studying the properties of electron transport, there are still many things that could be studied further, such as dual inter-dot coupling effects and the magnetic effect on two-state coupled QDs .

---

<sup>1</sup> Only when the interaction between same states: *odd-odd*( $v_{db}$ ) and *even-even*( $v_{ca}$ ) coupling.

## References

- [1] A. Yacoby, M. Heiblum, and D. Mahalu, and Hadas Shtrikman, Phys. Rev. Lett. **74**, 4047(1995).
- [2] C. Livermore, C. H. Crouch, R. M. Westervelt, K. L. Campman, and A. C. Gossard, Science **274**, 1332 (1996).
- [3] M. L. Ladrón de Guevara, F. Claro, and Pedro A. Orellana, Phys. Rev. B **67**, 195335 (2003).
- [4] M. Sigrist, A. Fuhrer, T. Ihn, K. Ensslin, S. E. Ulloa, W. Wegscheider, and M. Bichler, Phys. Rev. Lett. **93**, 066802 (2004).
- [5] Y. S. Joe, E. R. Hedin, and A. M. Satanin, Phys. Rev. B **76**, 085419 (2007).
- [6] Y. Aharonov and D. Bohm, Phys. Rev. **115**, 485 (1959).
- [7] A. W. Holleitner, C. R. Decker, H. Qin, K. Eberl, and R. H. Blick, Phys. Rev. Lett. **87**, 256802 (2001).
- [8] G. Breit and E. Wigner, Phys. Rev. **49**, 519 (1936).
- [9] U. Fano, Phys. Rev. **124**, 1866 (1961).

- [10] J. Kim, *Electron transport through the double quantum dots in Aharonov-Bohm rings*, Master Thesis, Department of Physics and Astronomy, Ball State University, Muncie, Indiana (2005).
- [11] E. R. Hedin, Y. S. Joe, and A. M. Satanin, *J. Comput. Electron.* **7**, 280 (2008).
- [12] S. Datta, *Electronic Transport in Mesoscopic Systems*, Chap. 1, Cambridge Univ. Press, Cambridge, (1995).
- [13] U. F. Keyser, *Nanolithography with an atomic force microscope: quantum point contacts, quantum dots, and quantum rings*, PhD dissertation, Universität Hannover, Germany (2000).
- [14] D. J. Griffiths, *Introduction to Quantum Mechanics*, Pearson Prentice Hall (2005).
- [15] Y. Imry and R.A. Webb, *Scientific American* **260** , 56 (1989).
- [16] R. Landauer, *IBM J. Res. Dev.* **1**, 223 (1957).
- [17] P. J. Price, *Phys. Rev. B* **38**, 1994 (1988).
- [18] Z. Shao and W. Porod, *Phys. Rev. B* **51**, 1931 (1995).
- [19] W. Porod, Z. Shao, and C. S. Lent, *Phys. Rev. B* **48**, 8495 (1993).
- [20] J. Leo and G. A. Toombs, *Phys. Rev. B* **43**, 9944 (1991).

- [21] A. Platt, *Fano resonance in two-dimensional quantum wires with an offset attractive impurity*, Master Thesis, Ball State University, Muncie, Indiana (2004).
- [22] N. W. Ashcroft and N. D. Mermin, *Solid State Physics*, Holt, Rinehart and Winston (1976).
- [23] C. Kittel, *Introduction to Solid State Physics*, Wiley (2004).
- [24] A. W. Holleitner, R. H. Blick, A. K. Hüttel, K. Ebert and J. P. Kotthaus, *Science* **297**, 70 (2002).
- [25] C. W. J. Beenakker, *Phys. Rev. B* **44**, 1646 (1991).
- [26] B. Kubala and J. König. *Phys. Rev. B* **65**, 245301 (2002).
- [27] J. C. Chen, A. M. Chang, and M. R. Melloch, *Phys. Rev. Lett.* **92**, 176801 (2004).
- [28] V. Kashcheyevs, A. Schiller, A. Aharony, and O. Entin-Wohlman, *Phys. Rev. B* **75**, 115313 (2007).

## Appendix A

### Calculation of the transmission amplitude for single-state QD.

For ( $n = -1$ ), Eq. (4.2) would be changed to

$$-[V_0\psi_{-2} + V_1e^{-i\varphi/4}\psi_A + V_1e^{i\varphi/4}\psi_B] + \varepsilon_{-1}\psi_{-1} = E\psi_{-1}. \quad (\text{A.1})$$

Since the wavefunctions  $\psi_n = e^{i\theta n} + re^{-i\theta n}$  for  $n < 0$  and  $\psi_n = te^{i\theta n}$  for  $n \geq 1$ , Eq. (A.1)

becomes,

$$-V_0(e^{-2i\theta} + re^{2i\theta}) - V_1e^{-i\varphi/4}\psi_A - V_1e^{i\varphi/4}\psi_B + (\varepsilon_{-1} - E)(e^{-i\theta} + re^{i\theta}) = 0. \quad (\text{A.2})$$

Eq. (A.2) can be simplified to

$$[-V_0e^{2i\theta} + (\varepsilon - E)e^{i\theta}]r - V_1e^{-i\varphi}\psi_A - V_1e^{i\varphi}\psi_B = V_0e^{-2i\theta} - (\varepsilon - E)e^{-i\theta}. \quad (\text{A.3})$$

We could more simplify Eq. (A.3) by using the dispersion relation introduce in Eq.(3.15):

$$E = -2V_0 \cos\theta + \varepsilon = -V_0(e^{i\theta} + e^{-i\theta}) + \varepsilon. \quad (\text{A.4})$$

Multiplying by  $e^{\pm i\theta}$  to both sides of Eq. (A.4) leads to

$$V_0 = -V_0e^{-2i\theta} + (\varepsilon - E)e^{-i\theta} \quad \text{or} \quad V_0 = -V_0e^{2i\theta} + (\varepsilon - E)e^{i\theta}. \quad (\text{A.5})$$

So we could take advantage of Eq. (A.5) to simplify Eq. (A.3):

$$V_0 r - V_1 e^{-i\varphi/4} \psi_A - V_1 e^{i\varphi/4} \psi_B = -V_0 . \quad (\text{A.6})$$

For  $n=\text{dot A}$ , we could also start to use Eq. (4.2):

$$-V_1 e^{i\varphi/4} \psi_{-1} - V_1 e^{-i\varphi/4} \psi_1 - v_j \psi_B + \varepsilon_A \psi_A = E \psi_A . \quad (\text{A.7})$$

Using wavefunctions appropriately leads to

$$-V_1 e^{i\varphi/4} (e^{-i\theta} + r e^{i\theta}) - V_1 e^{-i\varphi/4} t e^{i\theta} - v_j \psi_B + (\varepsilon_A - E) \psi_A = 0 . \quad (\text{A.8})$$

We can re-arrange Eq. (A.8):

$$-V_1 e^{i\varphi/4} e^{i\theta} r - V_1 e^{-i\varphi/4} e^{i\theta} t + (\varepsilon_A - E) \psi_A - v_j \psi_B = V_1 e^{i\varphi/4} e^{-i\theta} . \quad (\text{A.9})$$

For ( $n=\text{dot B}$ ), the procedure to derive the final equation is the same as for dot A (Eq. (A.9)). So the final form is given as

$$-V_1 e^{i\varphi/4} e^{i\theta} r - V_1 e^{-i\varphi/4} e^{i\theta} t + v_j \psi_A - (\varepsilon_A - E) \psi_B - v_j \psi_A = V_1 e^{i\varphi/4} e^{-i\theta} . \quad (\text{A.10})$$

For ( $n=1$ ), we have

$$-V_1 e^{i\varphi/4} \psi_A - V_1 e^{-i\varphi/4} \psi_B - V_0 t e^{2i\theta} + \varepsilon \psi_1 = E \psi_1 . \quad (\text{A.11})$$

Since  $\psi_1 = t e^{i\theta}$  for  $n=1$ ,

$$-V_1 e^{i\varphi/4} \psi_A - V_1 e^{-i\varphi/4} \psi_B - V_0 t e^{2i\theta} + (\varepsilon - E) e^{i\theta} t = 0 . \quad (\text{A.12})$$

Re-arranging it after the dispersion relation is used gives,

$$V_0 t - V_1 e^{i\varphi/4} \psi_A - V_1 e^{-i\varphi/4} \psi_B = 0 \quad (\text{A.13})$$

Now, we have four equations [Eqs. (A.6), (A.9), (A.10), and (A.13)] and four unknowns.

It is convenient to display these equations in the form of a **matrix**. Suppose that we can control all parameters in the equations except  $t, r, \psi_A$  and  $\psi_B$  which will be solved for:

$$\begin{pmatrix} V_0 & 0 & -V_1 e^{-i\varphi/4} & -V_1 e^{i\varphi/4} \\ -V_1 e^{i\varphi/4} e^{i\theta} & -V_1 e^{-i\varphi/4} e^{i\theta} & \varepsilon_A - E & -v_j \\ -V_1 e^{-i\varphi/4} e^{i\theta} & -V_1 e^{i\varphi/4} e^{i\theta} & -v_j & \varepsilon_B - E \\ 0 & V_0 & -V_1 e^{i\varphi/4} & -V_1 e^{-i\varphi/4} \end{pmatrix} \begin{pmatrix} r \\ t \\ \psi_A \\ \psi_B \end{pmatrix} = \begin{pmatrix} -V_0 \\ V_1 e^{i\varphi/4} e^{-i\theta} \\ V_1 e^{-i\varphi/4} e^{-i\theta} \\ 0 \end{pmatrix} \quad (\text{A.14})$$

Let the ‘M’ be a 4x4 matrix and ‘S’ and ‘C’ are 1x4 vectors :  $MS = C$ . According to the standard matrix rule,

$$S = M^{-1} C \quad (\text{A.15})$$

Therefore, finding  $S_{12}$  leads us to the transmission amplitude  $t(E, \varphi)$  :

$$t(E, \varphi) = \frac{-(e^{2i\theta} - 1)V_1^2 \{E - 2e^{2i\theta} v_j - \varepsilon_A + e^{4i\theta} (E - \varepsilon_B)\}}{e^{i(3\theta - 2\varphi)} V_1^4 + e^{3i(\theta + 2\varphi)} V_1^4 + 2e^{i\theta} V_1^2 v_j + 2e^{2i(\theta + 2\varphi)} V_1^2 v_j + e^{i(\theta + 2\varphi)} \{-2e^{2i\theta} V_1^4 + v_j^2 - (E - \varepsilon_A)(E - \varepsilon_B) - 2e^{i\theta} V_1^2 (2E - \varepsilon_A - \varepsilon_B)\}} \quad (\text{A.16})$$

## Appendix B

### Calculation on the transmission amplitude at $\varepsilon_A = -\varepsilon_B$

The transmission amplitude can be calculated along the yellow line in Fig. 4.16(a) when we borrow Eq. (A.14):

$$\begin{pmatrix} V_0 & 0 & -V_1 e^{-i\varphi} & -V_1 e^{i\varphi/4} \\ -V_1 e^{i\varphi} e^{i\theta} & -V_1 e^{-i\varphi} e^{i\theta} & \varepsilon_A - E & -v_j \\ -V_1 e^{-i\varphi} e^{i\theta} & -V_1 e^{-i\varphi} e^{i\theta} & -v_j & \varepsilon_B - E \\ 0 & V_0 & -V_1 e^{i\varphi} & -V_1 e^{-i\varphi} \end{pmatrix} \begin{pmatrix} r \\ t \\ \Psi_A \\ \Psi_B \end{pmatrix} = \begin{pmatrix} -V_0 \\ V_1 e^{i\varphi} e^{-i\theta} \\ V_1 e^{-i\varphi} e^{-i\theta} \\ 0 \end{pmatrix} \quad (\text{B.1})$$

where in the absence of magnetic flux ( $\varphi = 2\pi \frac{\Phi}{\Phi_0} = 0$ ) there are symmetric lead-dot couplings ( $V_1 = 0.3$ ). Then along the reverse diagonal yellow line  $\varepsilon_A + \varepsilon_B = 0$ , and the inter-dot coupling  $v_j = 0$  results in (where, at  $E=0$ ,  $e^{i\theta} = i$ ),

$$\begin{pmatrix} 1 & 0 & -V_1 & -V_1 \\ -V_1 i & -V_1 i & \varepsilon_A & 0 \\ -V_1 i & -V_1 i & 0 & -\varepsilon_A \\ 0 & 1 & -V_1 & -V_1 \end{pmatrix} \begin{bmatrix} r \\ t \\ \Psi_A \\ \Psi_B \end{bmatrix} = \begin{bmatrix} -1 \\ -V_1 i \\ -V_1 i \\ 0 \end{bmatrix} \quad (\text{B.2})$$

Next step is very straightforward. We can expand Eq. (B.2):

$$r - V_1 \Psi_A - V_1 \Psi_B = -1 \quad . \quad (\text{B.3})$$

The 2<sup>nd</sup> row is

$$-V_1 r i - V_1 t i + \varepsilon_A \psi_A = -V_1 i . \quad (\text{B.4})$$

The next one is

$$-V_1 r i - V_1 t i - \varepsilon_A \psi_B = -V_1 i . \quad (\text{B.5})$$

The last row becomes

$$t - V_1 \psi_A - V_1 \psi_B = 0 . \quad (\text{B.6})$$

Combining Eq. (B.4) and Eq. (B.5), we have

$$\varepsilon_A (\psi_A + \psi_B) = 0 , \quad (\text{B.7})$$

which leads us to

$$\psi_A + \psi_B = 0 \quad \text{when } \varepsilon_A \neq 0 . \quad (\text{B.8})$$

Using Eq. (B.8), Eq. (B.6) becomes

$$t - V_1 (\psi_A + \psi_B) = 0 . \quad (\text{B.9})$$

Since  $\psi_A + \psi_B = 0$  from Eq. (B.8),

$$t = 0 \quad (\varepsilon_A \neq 0, \varepsilon_A + \varepsilon_B = 0) . \quad (\text{B.10})$$

## Appendix C

Calculation of the transmission amplitude at  $(E, \varepsilon_A, \varepsilon_B) \rightarrow (0,0,0)$

Let us start by plugging  $(E, \varepsilon_A, \varepsilon_B) \rightarrow (0,0,0)$  into Eq. (B.1):

$$\begin{pmatrix} 1 & 0 & -V_1 & -V_1 \\ -V_1 i & -V_1 i & 0 & 0 \\ -V_1 i & -V_1 i & 0 & 0 \\ 0 & 1 & -V_1 & -V_1 \end{pmatrix} \begin{bmatrix} r \\ t \\ \Psi_A \\ \Psi_B \end{bmatrix} = \begin{bmatrix} 1 \\ -V_1 i \\ -V_1 i \\ 0 \end{bmatrix} \quad (\text{C.1})$$

It is very straightforward to simplify Eq. (C.1). We have three equations:

$$r - V_1 \Psi_A - V_1 \Psi_B = -1 \quad , \quad (\text{C.2})$$

$$-V_1 r i - V_1 t i = -V_1 i \quad , \text{ and} \quad (\text{C.3})$$

$$t - V_1 \Psi_A - V_1 \Psi_B = 0 \quad . \quad (\text{C.4})$$

Combining Eq. (C.2) and Eq. (C.3), we have

$$r - t = -1 \quad . \quad (\text{C.5})$$

Dividing both side of Eq. (C.3) by  $V_1$  and  $i$  leads us to

$$r + t = 1 \quad . \quad (\text{C.6})$$

From Eq. (C.5) and (C.6), now we know  $t = 1$  . Since the transmission  $T$  is written as

$T = |t|^2$ , transmission  $T$  becomes one ( $T=1$ ) .

## Appendix D

### Calculations of the transmission probability for two states in a coupled QD

Let us consider the solutions of the wave functions to be given as

$$\psi_n = e^{in\theta} + re^{-in\theta} \quad (n \leq 0) \quad (\text{D.1})$$

$$\psi_n = te^{in\theta}. \quad (n \geq 1) \quad (\text{D.2})$$

Applying the wave functions into the tight-binding Schrodinger equations (Eq. (4.2)) for six sites gives the following equations:

For  $n=0$ , Eq. (4.2) is changed to

$$-V_0\psi_{-1} - V_{al}e^{-i\varphi}\psi_a - V_{be}e^{-i\varphi}\psi_b - V_{dl}e^{i\varphi} - V_{cl}e^{i\varphi}\psi_c + (\varepsilon_0 - E)\psi_0 = 0. \quad (\text{D.3})$$

After the wavefunctions are substituted, Eq. (D.3) becomes

$$-V_0(\psi_0 e^{i\theta} - 2i \sin \theta) + (\varepsilon_0 - E)\psi_0 - V_{al}e^{-i\varphi}\psi_a - V_{bl}e^{-i\varphi}\psi_b - V_{dl}e^{i\varphi}\psi_d - V_{cl}e^{i\varphi}\psi_c = 0. \quad (\text{D.4})$$

We can rewrite Eq. (D.4) in terms of  $\psi_0, \psi_a, \psi_b, \psi_c, \psi_d$ , and  $t$ :

$$-(V_0 e^{i\theta} + E - \varepsilon_0)\psi_0 - V_{al}e^{-i\varphi}\psi_a - V_{bl}e^{-i\varphi}\psi_b - V_{cl}e^{i\varphi}\psi_c - V_{dl}e^{i\varphi}\psi_d = 2iV_0 \sin \theta. \quad (\text{D.5})$$

For  $n=a$ , applying the same steps for  $n=0$ , we have

$$-V_{al}e^{i\varphi}\psi_0 + (\varepsilon_a - E)\psi_a - v_{da}\psi_d - v_{ca}\psi_c - V_{ar}e^{-i\varphi}t = 0. \quad (\text{D.6})$$

For  $n=b$ , the final expression becomes

$$-V_{bl}e^{i\varphi}\psi_0 - V_{br}e^{-i\varphi}t - v_{cb}\psi_c - v_{db}\psi_d + (\varepsilon_b - E)\psi_b = 0. \quad (\text{D.7})$$

With the same procedures, we have other 3 equations for  $n=c$  and  $n=d$ :

$$-V_{cl}e^{-i\varphi}\psi_0 - V_{cr}e^{i\varphi}t - v_{ca}\psi_a - v_{cb}\psi_b + (\varepsilon_c - E)\psi_c = 0, \quad (\text{D.8})$$

$$-V_{dl}e^{-i\varphi}\psi_0 - V_{dr}e^{i\varphi}t - v_{da}\psi_a - v_{db}\psi_b + (\varepsilon_d - E)\psi_d = 0. \quad (\text{D.9})$$

And finally for  $n=1$ , we have

$$-V_{ar}e^{i\varphi}\psi_a - V_{br}e^{i\varphi}\psi_c - V_{cr}e^{-i\varphi}\psi_c - V_{dr}e^{-i\varphi}\psi_d + V_0e^{-i\theta}t = 0. \quad (\text{D.10})$$

We combine six equations from Eq. (D.5) to Eq. (D.10) and put them into the following matrix form to obtain the transmission amplitude:

$$\begin{pmatrix} V_0e^{-i\theta} & -V_{al}e^{-i\varphi} & -V_{bl}e^{-i\varphi} & -V_{cl}e^{i\varphi} & -V_{dl}e^{i\varphi} & 0 \\ 0 & -V_{ar}e^{i\varphi} & -V_{br}e^{i\varphi} & -V_{cr}e^{-i\varphi} & -V_{dr}e^{-i\varphi} & V_0e^{-i\theta} \\ -V_{al}e^{i\varphi} & \varepsilon_a - E & 0 & -v_{ca} & -v_{da} & -V_{ar}e^{-i\varphi} \\ -V_{bl}e^{i\varphi} & 0 & \varepsilon_b - E & -v_{cb} & -v_{db} & -V_{br}e^{-i\varphi} \\ -V_{cl}e^{-i\varphi} & -v_{ca} & -v_{cb} & \varepsilon_c - E & 0 & -V_{cr}e^{i\varphi} \\ -V_{dl}e^{-i\varphi} & -v_{da} & -v_{db} & 0 & \varepsilon_d - E & -V_{dr}e^{i\varphi} \end{pmatrix}$$

$$\times \begin{pmatrix} \psi_0 \\ \psi_a \\ \psi_b \\ \psi_c \\ \psi_d \\ t \end{pmatrix} = \begin{pmatrix} 2iV_0 \sin \theta \\ 0 \\ 0 \\ 0 \\ 0 \\ 0 \end{pmatrix} \quad (\text{D.11})$$

The general transmission amplitude  $t$  from Eq. (D.11) cannot be reduced to a simple form. Assuming that there is no direct inter-dot coupling ( $v_{da} = v_{db} = v_{cb} = v_{ca} = 0$ ) on magnetic flux ( $\Phi = 0$ ) in a symmetric ring ( $V_{la} = V_{lb} = V_{lc} = V_{ld} = V_{rd} = V_{rc} = V_{rb} = V_{ra} = V_1$ ),  $t$  is given as<sup>1</sup>

$$t = \frac{-2ie^{2i\theta}V_1^2\{4E^3 - \varepsilon_a\varepsilon_b\varepsilon_c - \varepsilon_a\varepsilon_b\varepsilon_d - \varepsilon_b\varepsilon_c\varepsilon_d - 3E^2(\varepsilon_a + \varepsilon_b + \varepsilon_c + \varepsilon_d) + 2E[\varepsilon_c\varepsilon_d + \varepsilon_b(\varepsilon_c + \varepsilon_d) + \varepsilon_a(\varepsilon_b + \varepsilon_c + \varepsilon_d)]\}\sin\theta}{E^4V_0 + V_0\varepsilon_a\varepsilon_b\varepsilon_c\varepsilon_d + E^3[8e^{i\theta}V_1^2 - V_0(\varepsilon_a + \varepsilon_b + \varepsilon_c + \varepsilon_d) - 2e^{i\theta}V_1^2\{\varepsilon_b\varepsilon_c\varepsilon_d + \varepsilon_a[\varepsilon_c\varepsilon_d + \varepsilon_b(\varepsilon_c + \varepsilon_d)]\}] + E^2(\dots\dots) + E(\dots\dots)} \quad (\text{D.12})$$

<sup>1</sup> The denominator of  $t$  in Eq. (5.2) is completed:

$$E^2(-6e^{i\theta}V_1^2(\varepsilon_a + \varepsilon_b + \varepsilon_c + \varepsilon_d) + V_0(\varepsilon_c\varepsilon_d + \varepsilon_b(\varepsilon_c + \varepsilon_d) + \varepsilon_a(\varepsilon_b + \varepsilon_c + \varepsilon_d))) + E(4e^{i\theta}V_1^2(\varepsilon_c\varepsilon_d + \varepsilon_b(\varepsilon_c + \varepsilon_d) + \varepsilon_a(\varepsilon_b + \varepsilon_c + \varepsilon_d)) - V_0\{\varepsilon_b\varepsilon_c\varepsilon_d + \varepsilon_a[\varepsilon_c\varepsilon_d + \varepsilon_b(\varepsilon_c + \varepsilon_d)]\})$$